[AMERICAN JOURNAL OF SCIENCE, VOL. 294, FEBRUARY, 1994, P. 137–172]

American Journal of Science

FEBRUARY 1994

LAMINATION DURING SILICA DIAGENESIS—EFFECTS OF CLAY CONTENT AND OSTWALD RIPENING

JINCAI CHANG and YANIS C. YORTSOS*
Petroleum Engineering Program,
Department of Chemical Engineering,
University of Southern California,
Los Angeles, California 90089-1211

ABSTRACT. As a result of silica diagenesis, silica-rich formations (the Monterey Formation in California) become highly laminated both with respect to mineralogy (quartz, opal-CT, opal-A, siliceous shale) and to physical properties (hardness, porosity, and permeability). The degree and patterns of lamination vary according to the detrital material content and to the extent of diagenesis. Several qualitative theories to interpret these processes have been proposed in the past. However, quantitative models are presently lacking.

In this paper, mathematical models are developed to describe the diagenetic sequence *opal-A to opal-CT* (and by extension *to quartz*) via a dissolution-reprecipitation mechanism. The models account for dissolution, nucleation, and precipitation of the various amorphous and crystalline phases. We explore possible self-organization mechanisms that may lead to rock lamination, including clay effects and particle coarsening. Molecular diffusion in the liquid phase is assumed to regulate layering. The models predict diagenetic lamination that can be used to explain field observations.

NOMENCLATURE

A = surface area of solid phase, L^2
A_i = specific surface area (area per unit pore volume), $i = 0$, 1 and 2, L^{-1}
C = silicic acid concentration, mole L^{-3}
C_r = solubility ratio between phases
C_s = silicic acid concentration at the solution-solid interface, mole L^{-3}
C_{eq} = equilibrium concentration, mole L^{-3}
D = diffusion coefficient, L^2T^{-1}
J = nucleation rate, T^{-1}
J_0 = nucleation constant, T^{-1}
J_{diff} = mass flux by diffusion, in eq (2), mole $L^{-2}T^{-1}$
J_{kin} = mass flux by reaction, in eq (2), mole $L^{-2}T^{-1}$
K = see C_{eq}
L = system length, L
N = number of particles per volume, L^{-3}

* To whom correspondence should be addressed.

R = gas constant, $L^2T^{-2}K^{-1}$
T = temperature, K
V = volume of the solution, L^3
ΔG = activation energy, mole L^2T^{-2}
$\overline{C}$ = bulk concentration of the solution, mole L^{-3}
a_r = dimensionless area
c = compressibility, $LM^{-1}T^2$
c_c = clay concentration, percentage
f_i = particle size distribution function
k = Boltzman's Constant, mole $L^2T^{-2}K^{-1}$
k_r = ratio of rate constant
k_+ = rate constant, mole $L^{-2}T^{-1}$
k_i = kinetic constants (i = 1, 2, 3, and 4)
m = mass per volume, mole L^{-3}
n = number of H_2O molecules per SiO_2 molecule
n = wave number
n_c = surface concentration of the SiO_2-H_2O complex
n_o = available active sites
n_o = pressure, $L^{-1}MT^{-2}$
q = flow velocity, LT^{-1}
r = particle radius, L
r_c = critical radius, L
s = dimensionless concentration
s^* = dimensionless size-dependent solubility
t = time, T
v = molecular volume L^3
x = spatial distance, L
z = dimensionless volume of a single particle
Ω = degree of supersaturation
α = dimensionless diffusion constant
β = dimensionless specific surface area
δ = thickness of the boundary layer around a solid, L
η = pressure solution factor
θ = dimensionless solid mass
λ = dimensionless constant related to convection strength
μ = viscosity, $ML^{-1}T^{-1}$
ν = dimensionless water content
ξ = dimensionless distance
ρ = molar density, mole L^{-3}
σ = interfacial tension, MT^{-2}
τ = dimensionless time
ϕ = porosity
ϕ = particle volume distribution
ψ = dimensionless radius
ω = eigenvalue in linear stability analysis

1. INTRODUCTION

The diagenesis of silica is a process of great importance to the formation of rocks of high silica content, such as the Monterey Formation in California. The source of silica is mostly biogenic, from the remains of diatoms and radiolaria (Bramlette, 1946). Although carbonates, such as dolomite and calcite, are also common in some parts of this formation, it is silica that dominates the composition. The discovery of oil and gas in the 1940's has raised great interest on the properties of this formation (Bramlette, 1946). In particular, during the past decade, great progress has been made in understanding the particular geological and geochemical characteristics with theoretical and experimental work (Kastner, Keene, and Gieskes, 1977; Isaacs, 1980, 1981, 1982, 1984a, b; Williams, Parks, and Crerar, 1985; Williams and Crerar, 1985; Dunham and Blake, 1987).

The biogenic silica, generally amorphous and with poor crystal lattice structure, is thermodynamically unstable. As a result, a diagenetic phase transformation occurs, from the amorphous toward the stable crystalline silica phase, quartz. In the process, intermediate phases, such as cristobalite and tridymite, are also formed. It is generally agreed that the transformation mechanism is "dissolution and reprecipitation," a process extensively studied (Isaacs, 1980; Williams, Parks, and Crerar, 1985). Key to this diagenetic sequence is the difference in surface energies associated with different crystallinities (ranging from low, for the amorphous opal-A, to high for the ordered quartz phase), which thus give rise to different solubilities. Solutions in equilibrium with opal-A are supersaturated with respect to opal-CT or quartz. As dissolution of the amorphous phase proceeds, the concentration of the dissolved silicic acid rises, eventually exceeds the solubilities of the various intermediate crystalline silica phases, and induces nucleation of a more ordered crystalline phase. The growth of the latter persists until the amorphous phase has been completely dissolved.

It has been observed that the Monterey Formation is at several locations highly laminated (layered) both in terms of mineralogy and physical properties (fig. 1). The corresponding layer thickness is variable, ranging from millimeters to meters. As an example, one may consider the structure at the Santa Maria Basin (Dunham and Blake, 1987). At the top, it consists mainly of siliceous and phosphatic shales. Gradually downward, opal-CT/clay shale alterations appear, and at the bottom of the formation, chert and clay shale banding dominates.

The origin of this lamination has triggered much interest. A convenient and rather popular approach has been to attribute it directly to variations in initial sedimentation conditions. For example, one argues that depositional environments are directly affected by the climate, which changes in cycles (Pisciotto and Garrison, 1981; Isaacs, 1983). The accumulation of detrital materials on the ocean floor results from heavy rainfall; cold weather causes lower rates of diatom deposition. Hence, the

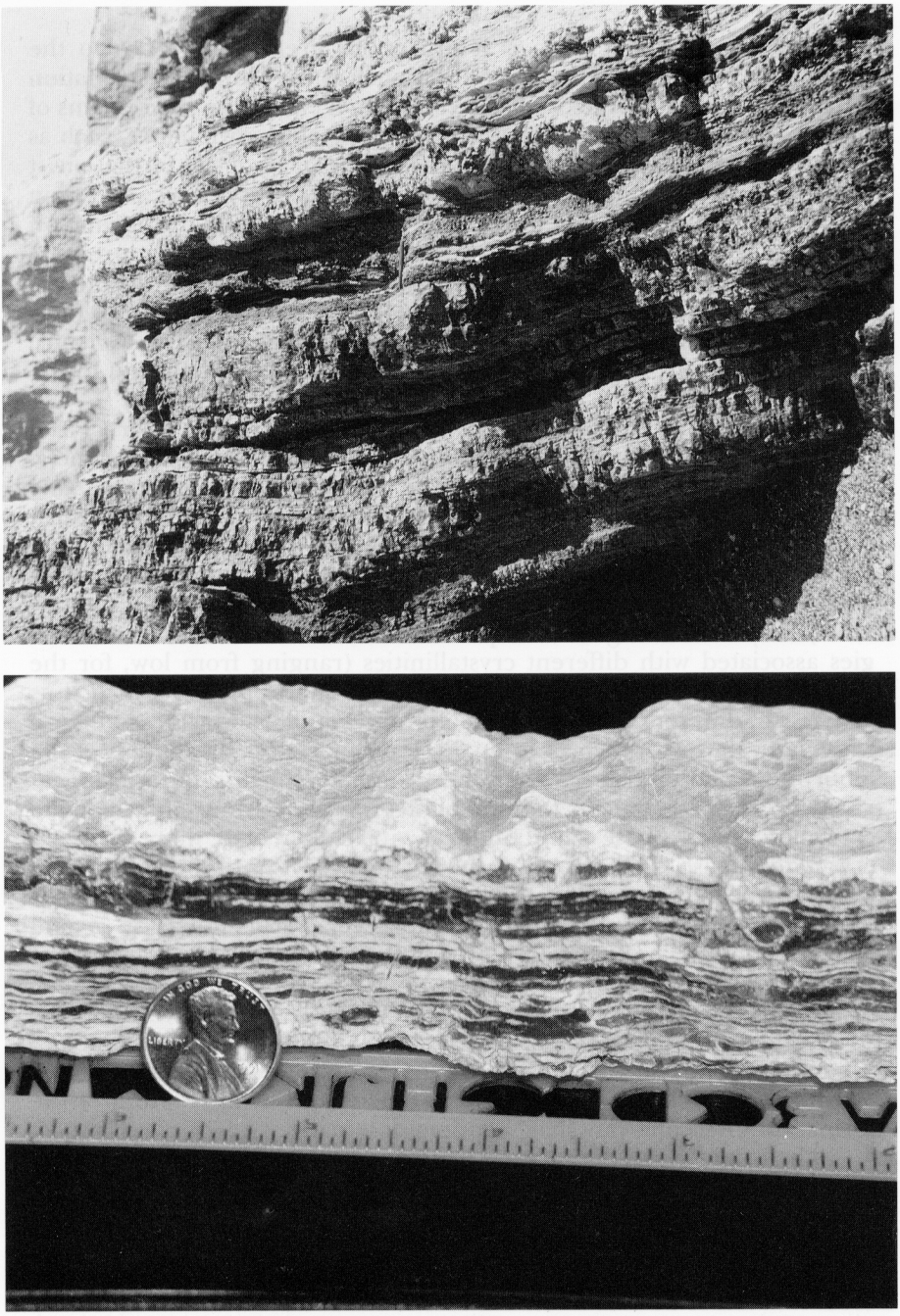

Fig. 1. Lamination at different scales (the height of the outcrop in the top picture is about 1.8 m).

argument goes, the final sediment is layer-like, each layer with a different silica/clay ratio.

Recent theoretical developments in related processes have suggested alternative methods. In contrast to previous developments, where a strong *external* input is required, these approaches attribute pattern development to *internal* process dynamics. Many unstable systems have been shown to possess an inherent capacity to self-organization, which is triggered by only mild weak variations in the initial conditions (Stern, 1954; Fliker and Ross, 1974; Keller, 1980, 1981; Venzl and Ross 1982; Ortoleva, 1983, Dee, 1986; Venzl, 1986a, b; Ortoleva and others, 1987a, b; Morse and Casey, 1988). The diagenesis of silica involves several key steps that are unstable. It is conceivable, therefore, that the lamination observed in the field is a consequence of such instabilities, which may drive the formation of spatial patterns.

We put forward two arguments that favor the interpretation of lamination in terms of internal dynamics. Kastner, Keene, and Gieskes (1977) have observed that opal-CT nucleation is more difficult in a clay-rich as opposed to a detrital-free, carbonate sediment environment. Given a diffusion mechanism, the dissolved silica would precipitate in clay-lean positions, where nucleation is more favorable (see also Isaacs, 1982). Because small amounts of clay are known to enhance pressure solution (de Boer, Nagtegaal, and Duyvis, 1977), silica in the clay-rich zone would dissolve faster, creating gradients in the concentration of the silicic acid which diffuses toward and precipitates in the clay-lean zone. This mechanism has a positive feedback, leading to the development of layers and lamination (Brueckner, Snyder, and Boudreu, 1987).

A second argument, proposed in related contexts (Feeney and others, 1983), attributes the formation of bands to Ostwald-ripening, where due to different surface energies and solubility, larger particles grow at the expense of continuously dissolving smaller ones. Weak perturbations on initial sizes can be amplified manyfold by such unstable mechanism, and, in the presence of diffusions, the competition between particles gives rise to spatial patterns. The final banding varies with the strength of diffusion, silica mass, temperature, and other factors.

These two hypotheses will be explored quantitatively in this paper in order to examine their relevance as possible lamination mechanisms in silica diagenesis. For this purpose, we develop a mathematical model of the dissolution-precipitation scheme using a continuum formalism. Although more phases are certainly present in real cases, for simplicity we consider here only two solid phases (one amorphous and one crystalline). Local rates of dissolution are assumed to be controlled kinetically, diffusion being of importance over larger scales. In the absence of more elaborate models, we shall make use of simple phenomenological relations to account for clay effects on both nucleation and pressure solution. Further refinements are certainly needed for a deeper understanding of these effects. The paper is organized as follows: First, the process is formulated in terms of a mathematical model. Then, the effects of clay

and particle coarsening (Ostwald ripening) on pattern development are analyzed with a numerical solution of the problem. Linear analysis is also used to identify the nature of the various instability mechanisms.

2. FORMULATION

The transformation of opal-A to opal-CT and quartz follows a dissolution-reprecipitation pathway that involves dissolution, nucleation and growth, according to the heterogeneous reaction sequence:

$$SiO_2 \cdot nH_2O \text{ (amorphous)} + 2H_2O \rightleftharpoons H_4SiO_4 + (n+2)\,H_2O \rightarrow SiO_2 \text{ (crystalline)} + (n+2)\,H_2O \quad (1)$$

The silicic acid in solution, H_4SiO_4, is the main dissolved species that diffuses in the aqueous phase.

In our formulation, we assume that the rock matrix initially consists of a mixture of amorphous silica and of some insoluble material, which includes clay or other detrital material. Upon precipitation, the newly formed crystals replace amorphous silica as the main constituent of the rock matrix. This takes place within the pore space of the compacting sediment. Subscripts 1 and 2 will be used to denote the two phases, amorphous and crystalline, respectively. While not generally appropriate, we take a porous media representation in terms of a collection of grain particles, the number N which remains constant during the dissolution process. These assumptions may be reasonable only at the early process stages, when the system porosity is high. Future refinements, perhaps in terms of a pore network (see Sharma and Yortsos, 1987), must be considered at later stages, when porosity becomes low and the grain model becomes inappropriate.

2.1. Dissolution-Growth

2.1.1. Local kinetic control.—The kinetics of silica dissolution and precipitation have been discussed in great detail in many publications (see Steefel and van Cappellen, 1990). Here, we proceed with a simple first-order reaction model, typically valid at neutral pH values and at relatively low concentrations. To account for both reaction and mass transfer, we consider the flat surface of figure 2. Let C_s be the silicic acid concentration at the interface, $\overline{C}$ the bulk concentration, and δ the boundary layer thickness where mass transfer occurs. The mass flux, for both dissolution and crystal growth, can be approximated as follows:

$$J \simeq \frac{D(C_s - \overline{C})}{\delta} \simeq \frac{k_+}{C_{eq}^{\infty}}(C_s - C_{eq}^{\infty}) \quad (2)$$

where C_{eq}^{∞} is the molar equilibrium concentration (mole/volume) with respect to the particular solid phase of a flat interface, and k_+ is the

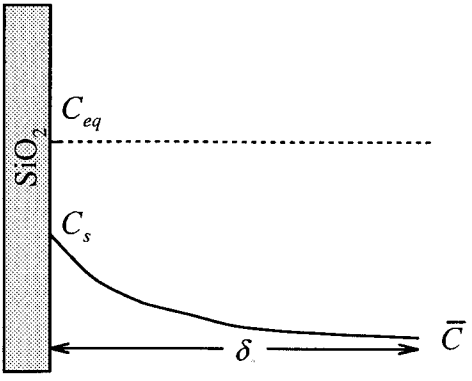

Fig. 2. Schematic of H_4SiO_4 concentration during dissolution.

reaction rate constant. Typical values of these parameters are given in table 1. Upon rearrangement, eq (2) becomes

$$J = \frac{k_+}{C_{eq}} \frac{(\overline{C} - C_{eq})}{\left(1 + \frac{\delta k_+}{DC_{eq}}\right)} \tag{3}$$

Whether the local process is under kinetic or mass transfer control is dictated by the dimensionless parameter $\delta k_+/DC_{eq}$. For the standard conditions $T = 50°C$, $D = 10^{-5}$ cm^2/s, and $\delta \leq 10^{-2}$ cm, the latter ratio is less than 1.9×10^{-7}, suggesting that surface reaction kinetics do indeed control the process locally. Kinetic control at the microscale has been suggested by many investigators in other related processes (Berner, 1980; Hurd, 1983). We note that effects of diffusion, which is paramount for pattern development, will be included in the formualtion at the macroscale.

Based on the above, a mass balance for a dissolving or growing particle of size r gives

$$\frac{\partial}{\partial t}\left(\rho \frac{4}{3} \pi r^3\right) \simeq 4\pi r^2 k_+ \left(\frac{C}{C_{eq}^{\infty}} - \frac{C_{eq}}{C_{eq}^{\infty}}\right) \tag{4}$$

or

$$\frac{dr}{dt} = \frac{k_+}{\rho}\left(\frac{C}{C_{eq}^{\infty}} - \frac{C_{eq}}{C_{eq}^{\infty}}\right) \tag{5}$$

where ρ is the molar density. Implicit above is the assumption of a size-independent rate constant k_+.

2.1.2. Solubility.—An important parameter in this formulation is the equlibrium solubility and its dependence on pressure solution and particle size. As pointed out in the Introduction, both crucially affect the growth pattern.

TABLE 1

Typical equilibrium and reaction constants at 50°C (from Rimstidt and Barnes, 1980)

Silica Phase	Solubility		Rate Constant k_+
	mol/cm^3	mg/kg	mol/cm^2 s
opal-A	3.05×10^{-6}	182.6	5.46×10^{-16}
opal-CT	8.14×10^{-7}	48.8	1.46×10^{-16}
quartz	2.50×10^{-7}	15.0	4.48×10^{-17}

A simplistic approach to modeling pressure solution effects is to introduce a pressure solution factor η that modifies the equilibrium concentration as follows

$$C^{\infty}_{eq,a} = \eta C^{\infty}_{eq} \tag{6}$$

where subscript a refers to "amorphous." This empirical factor is intended to capture clay effects on pressure solution. It has been observed that small amounts of clay can significantly affect pressure solution. The prevailing explanation is that clay layers between solid grains provide diffusion paths for the dissolved species (in this case H_4SiO_4), thereby accelerating dissolution (de Boer, Nagtegaal, and Duyvis, 1977). This mechanism operates at low values of clay content. Above a certain value (1 percent), however, the clay layer serves as a cushion instead, thus pressure solution is mitigated (de Boer, Nagtegaal, and Duyvis, 1977). Thus, η is expected to vary with clay content, c_c, according to the qualitative schematic of figure 3. This schematic is consistent, although it certainly does not fully explain field observations. For computational purposes only, the following

$$\eta \equiv f(c_c) = \frac{c_c}{Ac_c^2 + Bc_c + C} + D \tag{7}$$

will be used for this dependence. This is an ad-hoc assumption of little theoretical basis, and its only support is that it helps produce silica release rates consistent with the field observations, as discussed below. In the absence of a better alternative, this model will be used to describe clay pressure solution effects.

Because of the large specific area associated with small particles (< 1 μm) and surface irregularities of high curvature, effects of interfacial tension on the solubility are also important. For example, natural sediments of amorphous silica have specific surface areas in the range of 10 to 100 m^2/g (Williams, Parks, and Crerar, 1985, fig. 5). In fact, for mineral surfaces having a fractal geometry, as recently attributed to many natural systems, the value of the specific surface area is dramatically high (Feder,

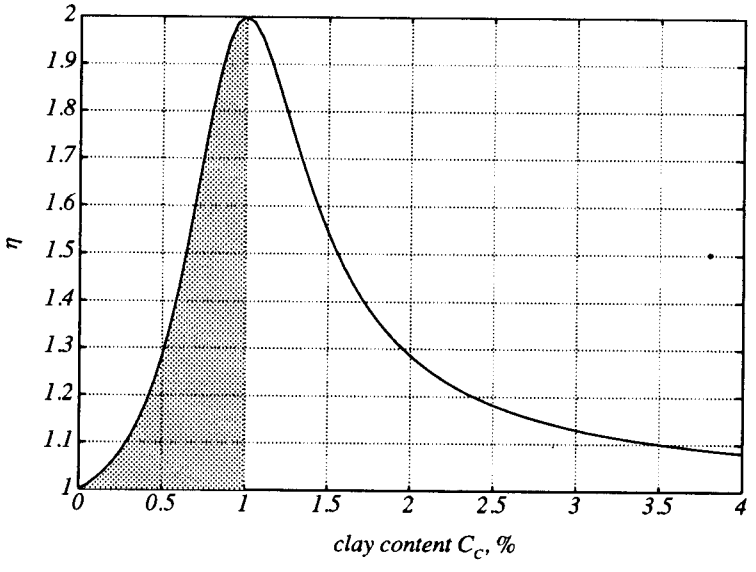

Fig. 3. Hypothetical schematic of the pressure solution factor η versus clay content.

1988). A relation between solubility $C_{eq}(r)$ and particle size r is given by Kelvin's equation

$$C_{eq}(r) = C_{eq}(\infty) \exp\left(\frac{2\sigma}{\rho RTr}\right) = C_{eq}(\infty) \exp\left(\frac{r^*}{r}\right) \tag{8}$$

where $C_{eq}(\infty)$, also denoted by C^{∞}_{eq}, is the solubility over a flat surface, and

$$r^* = \frac{2\sigma}{\rho RT} \tag{9}$$

The above two models, eqs (6) and (7), will be used to express the principal effects of solubility dependence.

2.2. Nucleation

The previous sections dealt with dissolution or growth. Precipitation is a two-step process also involving nucleation (see also Steefel and van Cappellen, 1990). The phenomenological approach to homogeneous nucleation is described in many references. For a given interfacial energy per unit area σ, the nucleation rate J is controlled by the degree of supersaturation $\Omega = C/C_{eq}$,

$$J = J_0 \exp\left[-\frac{\Delta G}{kT}\right] \tag{10}$$

where the activation energy for homogeneous nucleation G_{hom} is

$$\Delta G_{hom} = \frac{16\pi\sigma^3}{3[\rho RT \ln(\Omega)]^2} \tag{11}$$

Eq (11) contains two important variables, the degree of supersaturation Ω and the interfacial tension σ. Figure 4 is a plot of the nucleation rate versus supersaturation. It is apparent that for homogeneous nucleation to begin, a rather high critical supersaturation must be reached. Under normal diagenetic conditions, this critical value is seldom reached. For example, for an amorphous silica-water solution in equilibrium at 50°C, the SiO_2 solubility corresponding to a flat surface is 182.6 mg/kg. At the same temperature, the equilibrium solubility for the more crystalline opal-CT is 48.8 mg/kg, thus the degree of supersaturation with respect to opal-CT is $\Omega = 182.6/48.8 = 3.7$. For the typical values $J_0 = 10^{30}$ nuclei/cc-s, $\sigma = 180$ mJ/m^2, and $\rho = 2.5/60$ mole-cc, the calculated homogeneous nucleation rate at 50°C is $J = 10^{-410.6}$ nuclei/cc-s, clearly an infinitesimally small rate. Although an increase in temperature can dramatically increase homogeneous nucleation rates, it is more likely that, in natural environments, heterogeneous nucleation is the operating mechanism. Indeed, in the presence of favorable substrate surfaces, the activation energy required is much smaller than for the homogeneous case, and nucleation becomes much easier. Other factors, such as defects

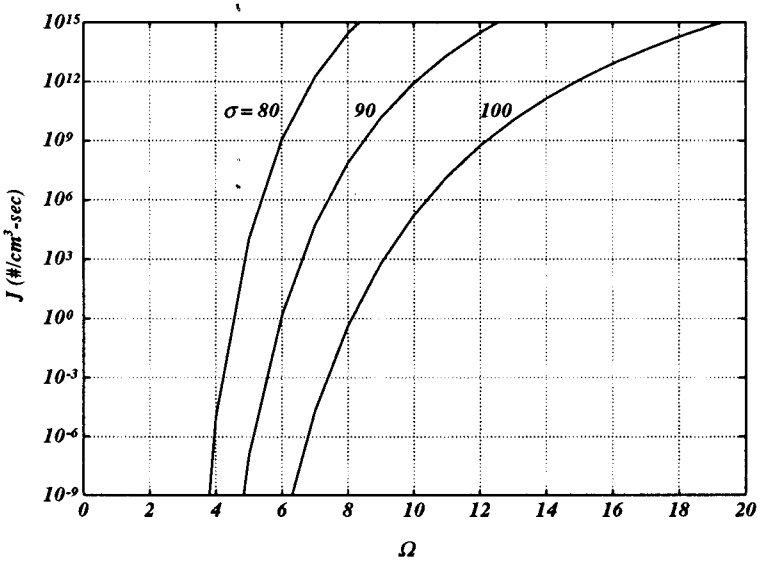

Fig. 4. Homogeneous nucleation rate versus supersaturation for various values of the interfacial tension in units of mJ/m^2 ($T = 50$°C and $J_0 = 10^{30}$ nuclei/cc-s.)

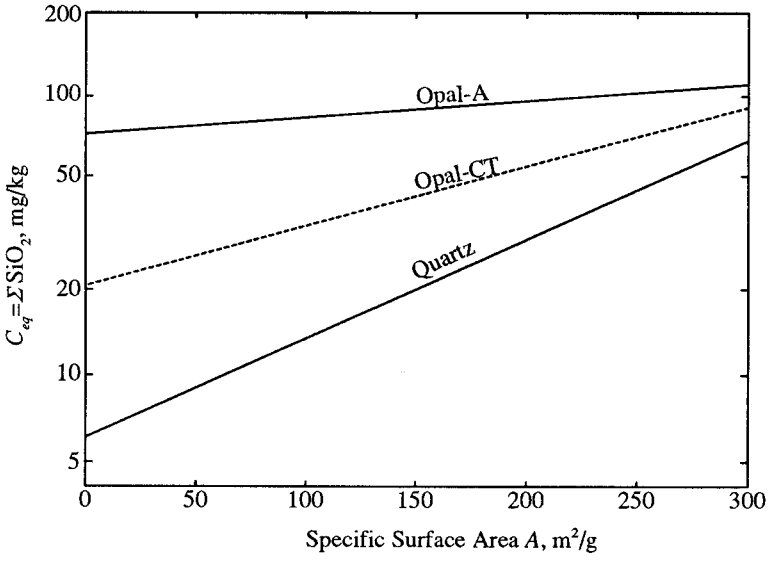

Fig. 5. Solubility versus specific surface area at $T = 25°C$ (reproduced from Williams, Parks, and Crerar, 1985).

on solid surfaces may also affect the nucleation rates substantially (Walton, 1967).

In a sediment environment, heterogeneous nucleation may be related to factors, such as clay content, Mg^{2+}, salinity, et cetera. Kastner, Keene, and Gieskes (1977) have experimentally demonstrated that when carbonate and magnesium ions are present, magnesium hydroxide precipitates are formed, which can serve as heterogeneous nucleation sites for the subsequent nucleation of opal-CT. In the presence of clay particles such as smectite, on the other hand, the formation of $Mg(OH)_2$ is retarded, and no opal-CT phase was detected in the experiments (Kastner, Keene, and Gieskes, 1977). Based on such observations, one may postulate that nucleation rates are clay-dependent, perhaps through the interfacial energy σ. The detrital content being variable with spatial position, the rate of nuclei formation at each position would differ accordingly. We may postulate a simple linear relation between clay content c_c and interfacial tension σ to regulate clay effects on nucleation rates

$$\sigma_a = \sigma_a(c_c) = ac_c + b \tag{12}$$

In view of the large sensitivity of the nucleation rate to σ, the values of the empirical parameters a and b and the spatial clay distribution would largely determine the rate of nuclei generation. Equivalently, eq. (12) can be interpreted as a means of altering $\Delta G = \alpha(c_c)\Delta G_{\text{hom}}$, via the factor $\alpha(c_c)$.

It must be pointed out that the dependence of nucleation on substrate surfaces and solution chemistry is at least very complicated. Clay may suppress nucleation of opal-CT, but on the other hand, it accelerates the transformation of opal-CT to quartz (Isaacs, 1982). Presence of Al^{3+} ions can greatly reduce the concentration of H_4SiO_4, yet low aluminum concentrations are favorable in forming quartz (Iler, 1979). In addition, the pre-exponential factor J_0 may well be different in heterogeneous and homogeneous nucleations and may be dependent on a variety of factors (see Steefel and van Cappellen, 1990 for an in-depth discussion). Many of these effects would lead to variations in J_0 and ΔG with clay content. These are not captured by eq (12), the main purpose of which is to modulate the clay dependence. Certainly, additional work is necessary for a clearer understanding of the role of clay effects on nucleation.

2.3. Mass Balances

We next proceed with deriving mass balances for the two conserved species, total silica and water. The general formalism is described in (Chang 1991). Here, we consider its reduction to a 1-D system in the absence of fluid flow effects. The total silica balance is

$$\frac{\partial(\phi C)}{\partial t} = D\frac{\partial^2(\phi C)}{\partial x^2} - \frac{\partial m_1}{\partial t} - \frac{\partial m_2}{\partial t} \tag{13}$$

where m_i denotes moles of phase i per total volume. For the rates of change we shall use continuum models. If A_1 denotes the specific surface area of amorphous particles (area/solution volume), then

$$\frac{\partial m_1}{\partial t} = A_1 k_{+1}\phi(C/C_{\text{eq1}} - \eta) \tag{14}$$

For the amorphous phase, A_1 is obtained as

$$A_1 = 4\pi N r_1^2(x, t) \tag{15}$$

where N refers to the number of particles per solution volume. The variation of r_1 is subject to the kinetics eq (5)

$$\dot{r}_1 = \frac{k_{+1}}{\rho_1 C_{eq1}^{\infty}}(C - C_{eq1}(r)) \tag{16}$$

For the rate of change of phase 2 we must allow for both nucleation and growth

$$\frac{\partial m_2}{\partial t} = \frac{4}{3}\pi r_c^3 J \rho_2 \phi + k_{+2} A_2 \phi(C/C_{\text{eq2}} - 1) \tag{17}$$

where J is determined from eqs (10) to (12). Now, however, the interfacial area A_2 cannot be simply expressed as in eq (15), the particle size distribution being no longer uni-modal. We must attach an index to any

particle to denote the time t' at which it was first nucleated, $r_2 = r_2(x, t, t')$, $t \geq t'$. Then, the rate expression is

$$\frac{\partial r_2}{\partial t} = \frac{k_{+2}}{\rho_2}\left(\frac{C}{C^{\infty}_{eq2}} - \frac{C_{eq2}(r)}{C^{\infty}_{eq2}}\right) \qquad t > t' \tag{18}$$

with the initial condition $r_2(x, t', t') = r_c(x, t')$. By simple superposition, we obtain the following expressions for the area of phase 2

$$A_2 = 4\pi \int_0^t r_2^2(x, t, t')J(x, t')\phi(t')\, dt'. \tag{19}$$

and for its mass

$$m_2 = \frac{4}{3}\pi\rho_2 \int_0^t r_2^3(x, t, t')J(x, t')\phi(t')\, dt' \tag{20}$$

The aqueous mass balance satisfies

$$\frac{\partial(\rho_l\phi)}{\partial t} + \frac{\partial m_{H_2O}}{\partial t} = 0 \tag{21}$$

where $\partial m_{H_2O}/\partial t$ is the rate of gain of net H_2O mass during dissolution of the amorphous phase eq (1)

$$\frac{\partial m_{H_2O}}{\partial t} = n\frac{\partial m_1}{\partial t} \tag{22}$$

Changes in porosity, compaction, and compressibility can also be readily incorporated (Chang, 1991).

2.4. Dimensionless Formulation

The above can be cast into a dimensionless notation by defining dimensionless concentration $s = C/C^{\infty}_{eq1}$, length $\xi = x/L$, time $\tau = t/\bar{t}$, radii $\psi_1 = r_1 r^*$, and $\psi_2 = r_2/r^*$ and phase contents $\theta_1 = m_1/\bar{m}$ and $\theta_2 = m_2/\bar{m}$, where $r^* = 2\sigma_1/\rho_1 RT$, $\bar{t} = \rho_1 r^*/k_{+1}$, and $\bar{m} = \rho_1 A_0 r^*$. In the above, time was taken to characterize the growth or dissolution of a characteristic particle size, L is the system size, while subscript "0" refers to initial conditions. The various dimensionless groups that arise are listed in table 2. Parameter α, in particular, is related to the inverse of the Thiele modulus commonly used in reaction engineering (see Lapidus and Amundson, 1977).

Upon rearrangement, the previous equations read

$$\frac{\partial s}{\partial \tau} = \alpha\beta\frac{\partial^2 s}{\partial \xi^2} - \beta\left(\frac{\partial \theta_1}{\partial \tau} + \frac{\partial \theta_2}{\partial \tau}\right) \tag{23}$$

$$\frac{\partial \theta_1}{\partial \tau} = a_{r1}(s - \eta) \tag{24}$$

$$\frac{\partial \theta_2}{\partial \tau} = a_{r2}\phi(s - C_r) + j_0 j(s)\phi \tag{25}$$

$$\dot{\psi}_1(\xi, \tau) = s - \eta \tag{26}$$

$$\dot{\psi}_2(\xi, \tau, \tau') = (s - C_r)/\rho_\tau \tag{27}$$

If we further denote the density ratio by

$$\rho_r = \rho_1/\rho_2 \tag{28}$$

then the volumetric clay concentration is

$$c_c = \frac{v_c}{1 - \phi} = \frac{v_c}{m_1/\rho_1 + m_2/\rho_2 + v_c} = \frac{1}{1 + \dfrac{\overline{m}}{\rho_r v_c}(\theta_1 + \rho_r \theta_2)} \tag{29}$$

We note that the clay content is not necessarily constant but varies with θ_1 and θ_2. Therefore, η is also indirectly a function of θ_1 and θ_2. Finally, eqs (26) and (27) can be integrated to yield

$$\psi_1(\xi, \tau) = \psi_1(\xi, 0) + \int_0^\tau [s(\tau) - \eta]\, d\tau \tag{30}$$

$$\psi_2(\xi, \tau, \tau') = \sigma_2/\sigma_1\rho_r + \frac{1}{\rho_r}\int_{\tau'}^{\tau} [s(\tau) - C_r]\, d\tau \tag{31}$$

TABLE 2

Dimensionless groups for silica diagenesis.

$$\alpha = \frac{DC_{eq1}}{L^2 A_0 K_{+1}}$$

$$\beta = \frac{\overline{m}}{C_{eq1}} = \frac{\rho_1 A_0 r^*}{C_{eq1}}$$

$$\nu = \frac{\overline{m}n}{\rho_l} = \frac{\rho_1 A_0 r^*}{\rho_l} n$$

$$C_r = C_{eq2}/C_{eq1}$$

$$j_0 = \frac{\frac{4}{3}\pi\rho_2 r_c^3 J_0}{A_0 k_{+1}}$$

$$a_{r1} = A_1/A_0$$

$$a_{r2} = A_2/A_0$$

$$k_r = k_{+2}/k_{+1}$$

$$\rho_r = \rho_2/\rho_1$$

The above is a fairly compact formulation of the silica-diagenesis process. It includes dissolution, nucleation, growth, mass transfer, clay, and particle size effects. Key variables are the dimensionless groups α, β, j_0, η, and C_r. Diffusion is controlled by α (equivalently by the system length L). Nucleation is modulated by j_0, the functional dependence $j(s)$, and the presence of clay eqs (7) and (12). Finally, the phase transformation is regulated via C_r, which depends on both pressure solution and particle size through eqs (7) and (8). In the above, we have assumed constant temperature. As pointed out in the Introduction, lamination and layering can be explained in terms of spatial self-organization driven by clay effects in augmenting the pressure solution and in affecting nucleation rates or by ripening during particle growth. These two effects are separately considered in the following sections. An insight on whether such mechanisms do indeed lead to pattern formation can be provided by a linear analysis. Such an analysis can quantitatively support qualitative arguments (such as those in Brueckner, Snyder, and Boudreu, 1987), while it is also useful for the interpretation of the nonlinear numerical solution. Before presenting the numerical results, therefore, we consider the linear stability predictions.

3. CLAY EFFECTS ON LAMINATION

We first consider effects of clay on lamination and spatial patterns. We proceed with the formulation of the previous section, with the further simplification that particle size effects on solubility are neglected, thus $C_{eq} = C_{eq}^{\infty}$.

3.1. Linear Stability

We analyze the stability of a spatially uniform base state during diagenesis by following the development of a small perturbation. If the perturbation decays, the uniform base state is stable, and there will be no tendency for pattern formation. Inversely, the perturbation will grow, possibly toward a new equilibrium state, in self-organizing systems. Before proceeding further we note that

$$\frac{\partial \eta}{\partial \theta_1} = \frac{\partial \eta}{dc_c} \cdot \frac{\partial c_c}{\partial \theta_1} = \dot{\eta}\varphi \tag{32}$$

and

$$\frac{\partial \eta}{\partial \theta_2} = \rho_r \dot{\eta}\varphi \tag{33}$$

where

$$\varphi = -\frac{\rho_1 v_c \overline{m}}{[\overline{m}(\theta_1 + \theta_2 \rho_r) + \rho_1 v_c]^2} < 0 \tag{34}$$

Therefore, the sign of the two derivatives is controlled by the dependence of η on the clay content, $\dot{\eta}$. For the present model, this can

take both positive and negative values (fig. 3). Following normal modes, all variables y_i (where $i = 1, 2, 3, 4, 5, 6$ stands for s, ψ_1, ψ_2, a_{r1}, a_{r2}, θ_1, and θ_2, respectively) are expressed in the form $y_i = y_{i,0} + \epsilon \sin(n\pi\xi) \exp(\omega\tau)$. Substitution into eqs (23) to (27) yields a linear set, for a non-trivial solution of which to exist, a (fourth order) eigenvalue condition in ω must be satisfied (Chang, 1991). Of most interest is the behavior at large values of n (small wavelengths), which, in the case of instability, would dominate the final pattern. In this limit, it can be shown that there exist one large negative root $\omega \to -\infty$, one vanishingly small root $\omega \to 0$, and two roots that satisfy (Chang, 1991)

$$\omega^2 + \phi\omega(a_{r1}\varphi\dot{\eta}) + \frac{2\psi_1}{\psi_{10}}\phi(s - \eta)\varphi\dot{\eta} = 0 \tag{35}$$

The second term above denotes effects of pressure solution only, while the third term reflects changes in the surface area. If we assume that area changes are secondary, $(\varphi\dot{\eta})^2 a_{r1}^2 \gg (8\psi_1/\psi_{10}^2)\dot{\eta}(s - \eta)$, the above admits one non-trivial solution

$$\omega \sim -\phi a_{r1}\varphi\dot{\eta} \tag{36}$$

Since $\varphi < 0$, it follows that large number wave instability (fine microlamination) develops when $\dot{\eta} > 0$ only, that, when the pressure solution increases with clay content. This is schematically summarized (see also Brueckner, Snyder, and Boudreu, 1987)

clay rich → more silica dissolved (pressure solution) →

higher clay content → further enhancement of dissolution.

When $\dot{\eta} < 0$, pressure solution alone is not sufficient for the development of pattern. Now, the coupling of surface area change must be also considered. Indeed, a small positive ω exists for $s < \eta$, that is, when the phase is dissolving (fig. 6). This effect, much weaker than pressure solution, favors long wave patterns (fig. 6). One concludes therefore, that a pressure solution-driven instability exists as long as the clay content is lower than a critical value (where $\dot{\eta} = 0$). For larger values, pressure solution effects may not be significant vis a vis microlamination

3.2. Numerical Solution

The final pattern depends of course on additional nonlinear effects and cannot be predicted simply by linear stability analysis alone. Therefore numerical simulations were performed next. Effects of diffusion were stressed, the sensitivity analysis being conducted by varying the values of α. The following four cases were simulated: (1) *Single phase only.* Here, there is no phase transformation, and only the effect of pressure solution is considered. (2) *Non-uniform nucleation, in the absence of pressure solution.* In this case, the interfacial tension is taken to be related to the clay content, but the pressure solution factor η was set to unity.

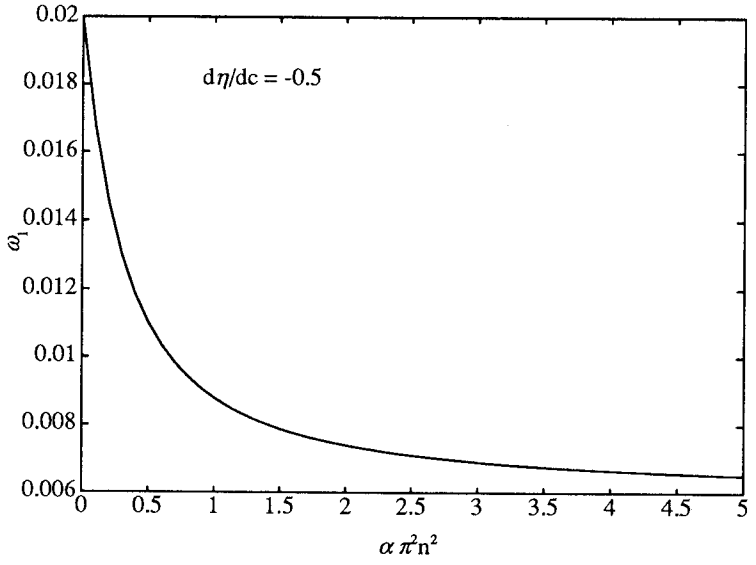

Fig. 6. Dominant eigenvalue versus wavenumber for $\dot{\eta} < 0$.

(3) *Uniform nucleation with pressure solution.* Here, the interfacial tension is assumed constant, thus the nuclei for the second phase are uniformly generated. (4) *Both the interfacial tension and the pressure solution are assumed to be related to the clay content.* Thus, a high clay concentration would both increase the dissolution rate and at the same time retard the nucleation rate.

In all simulations, the clay content was taken to vary in a small range in the region 0.20 to 0.25 percent, where $\dot{\eta}(c_c) > 0$. No-flux boundary conditions were used at the two ends. The initial condition was a small amplitude (less than 1 percent) sinusoidal or fBm (fractional Brownian motion) perturbation in clay content. fBm perturbations were used because they allow for correlations at all scales (Hurst, 1951; Mandelbrot and van Ness, 1968; Mandelbrot and Casey, 1988). The equations were discretized using central point differences, while a Newton-Raphson scheme was used to solve the nonlinear equations.

3.2.1. Case I: Pressure solution, no nucleation.—Results show that small initial variations in the clay content result in patterning of both clay and silica (fig. 7). Because no transformation of silica was considered here, however, the dissolved silica remains in solution, if below equilibrium levels, or it is redeposited as amorphous, if these levels are exceeded. Diffusion controls the wavelength of the patterns formed. For otherwise identical conditions, a longer wavelength pattern develops with strong diffusion (fig. 8A, $\alpha = 1.0$), whereas short wavelength patterns appear when the diffusion is much weaker (fig. 8B, $\alpha = 6.25 \times 10^{-4}$). The effect

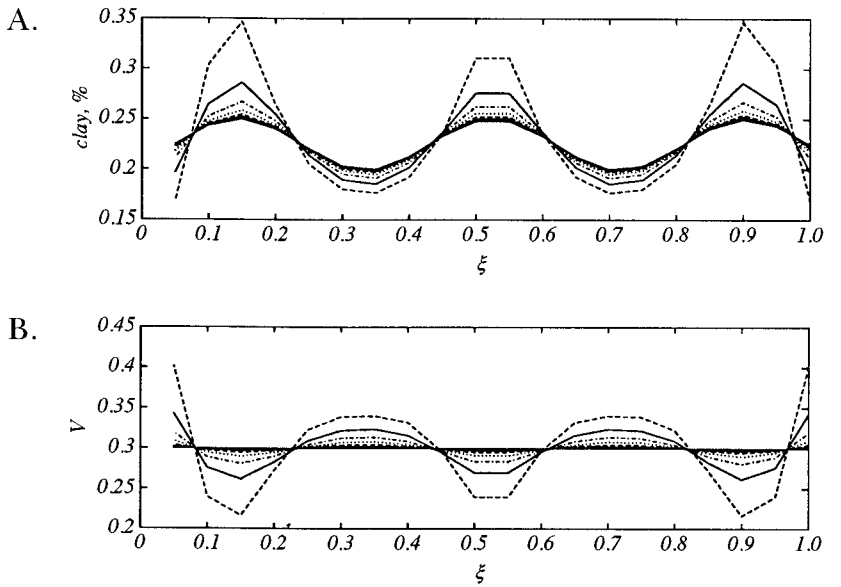

Fig. 7. Pressure solution effect on a single phase. (A) Relative clay content, (B) dimensionless silica content. ($\alpha = 2.5 \times 10^{-3}$, times $\tau = 0, 0.30, 1.4, 3.4, 6.5, 11, 16, 23.$)

of diffusion is predictable from the linear analysis, where it affects the rate of growth ω in the combination αn^2. Hence, one roughly expects the dependence $n \propto \alpha^{-1/2}$. The substantial difference between the nonlinear patterns of figure 8, both of which are based on the same initial (fBm) conditions, is indicative of the unstable nature of the system. When the clay content exceeds the critical value (1 percent), the instability mechanism due to pressure solution is suppressed. As predicted by the linear analysis, the mechanism due to the change of surface area now controls the pattern development. Patterns were still developed, although at a much smaller amplitude (Chang, 1991).

3.2.2. Case II: Nucleation, no pressure solution.—In the second set of simulations, σ was taken to vary linearly with the clay content in the range 40 to 70 mJ/m^2. A sinusoidal variation was used as the initial clay distribution (fig. 9A). Dissolution of the amorphous phase is independent of the clay content and solely proceeds due to solubility. From the nucleation kinetics of figure 4 it can be shown that nucleation proceeds rapidly in the low σ range ($\sigma = 40$ mJ/m^2). However, no nuclei are generated in the other end, $\sigma = 70$ mJ/m^2 (fig. 9C). Thus, crystal seeds would distribute "on and off" along the spatial direction depending on the clay concentration, which acts much like a filter (fig. 9C). The crystalline phase (opal-CT) grows at the respective positions (fig. 9D). In

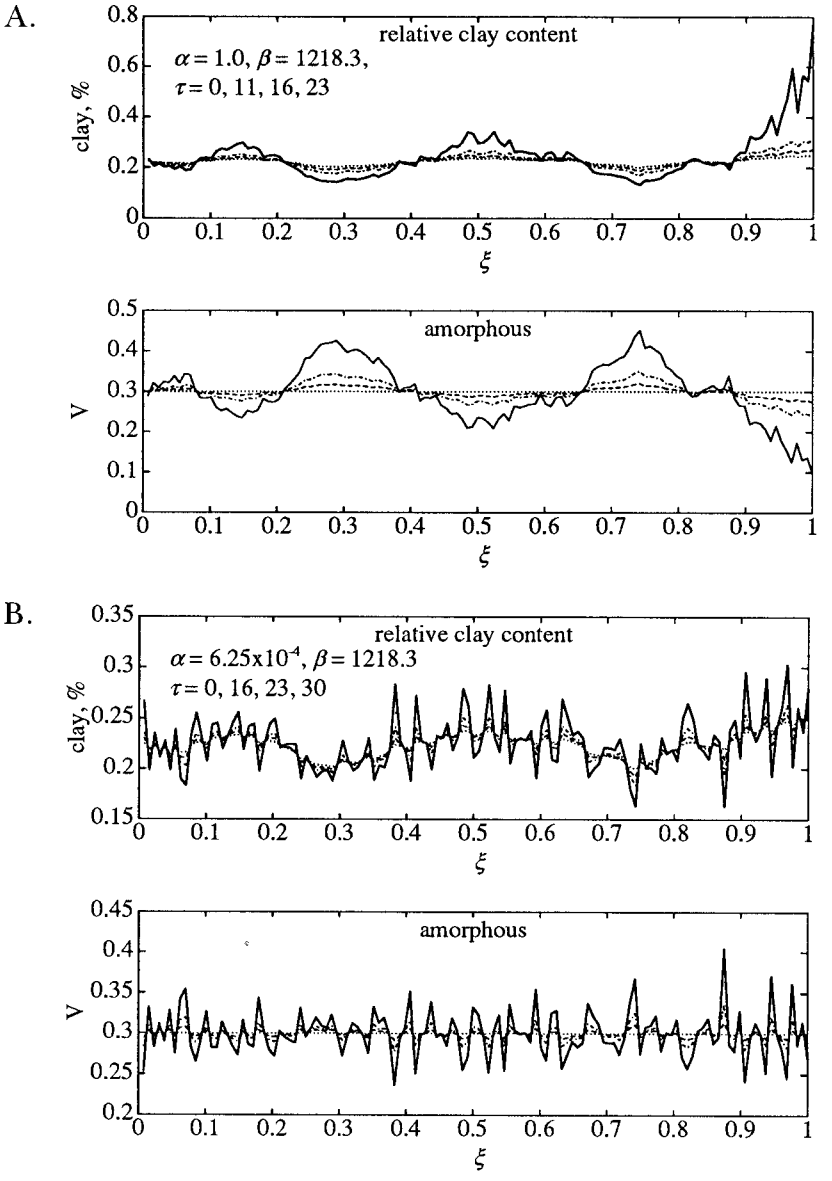

Fig. 8. Pressure solution on a single phase. (A) Strong diffusion ($\alpha = 1.0$, times $\tau = 0$, 11, 16, 23). (B) Weak diffusion ($\alpha = 6.25 \times 10^{-4}$, times $\tau = 0$, 16, 23, 30).

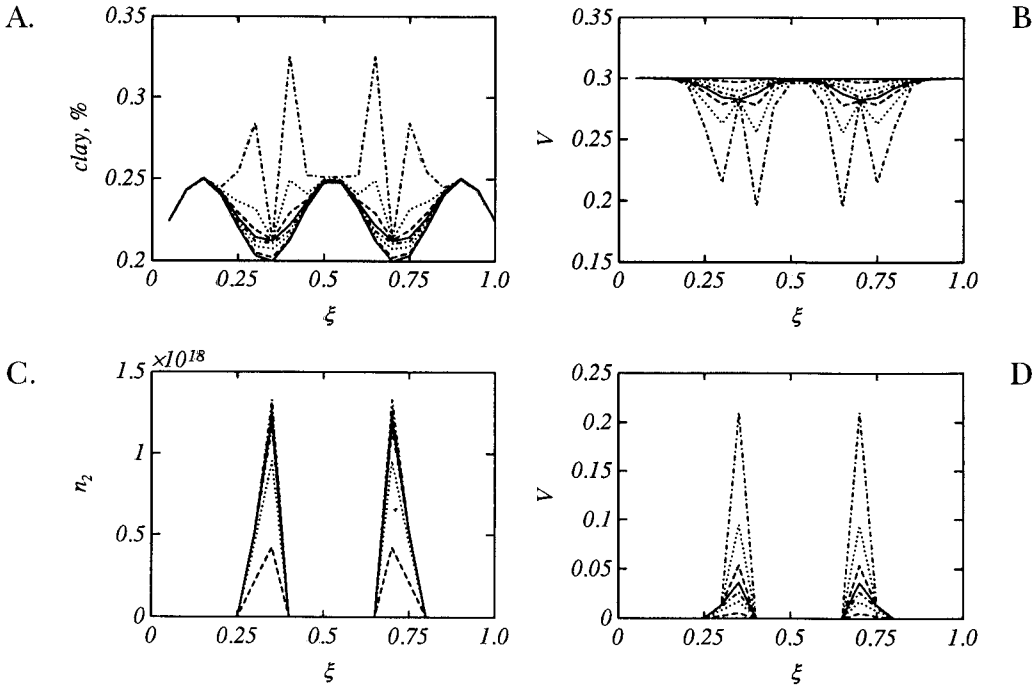

Fig. 9. Non-uniform nucleation, no pressure solution effect. (A) Relative clay content; (B) opal-A content; (C) total nuclei density; (D) opal-CT content. ($\alpha = 2.5 \times 10^{-3}$, times $\tau =$ 0, 0.30, 1.4, 3.4, 6.5, 11, 16, 23.)

the absence of pressure solution, the dissolution of opal-A is not directly related to the clay content, and it would otherwise have been spatially uniform. Because of its dependence on the growth of opal-CT, opal-A dissolves faster at early times when the formation of opal-CT results in lower concentrations of silic acid. At later times, as more and more solid deposits, both the dissolution rate of the first phase and the growth rate of the second phase slow down. Nonetheless, it was found numerically that opal-A still remains mostly at the positions of the nucleation peaks (fig. 9B, D). In this regard, the final pattern bears the signature of initial conditions (fig. 9B). It is precipitation that is affected by clay effects.

3.2.3. Case III: Pressure solution, no clay effects on nucleation.—Next, we considered the case in which phase transformation is allowed, the pressure solution factor η is in effect, but the interfacial tension is independent of the clay content. Hence, the nucleation rate is only affected by the concentration of the solution. An initial clay distribution identical to the previous was taken (fig. 10A). The dissolution of opal-A is directly affected by the clay content, thus the patterning of the first phase becomes more pronounced as the transformation proceeds. Because the formation of opal-CT consumes the mass rapidly, however, a strong

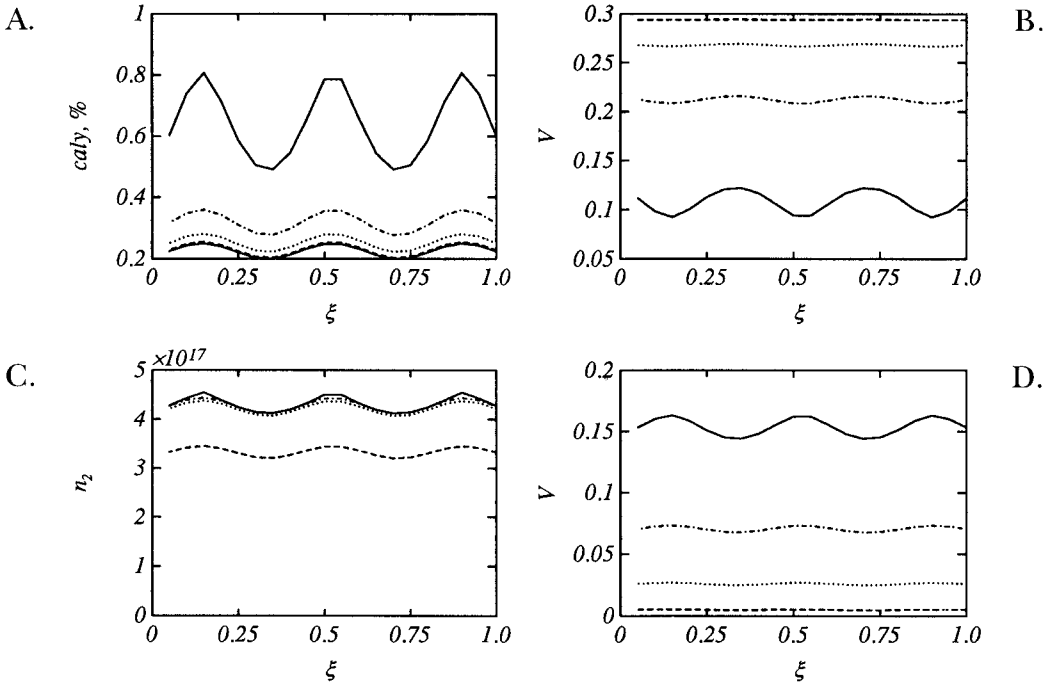

Fig. 10. Uniform nucleation with pressure solution. (A) Relative clay content; (B) opal-A content; (C) total nuclei density; (D) opal-CT content. $\sigma \equiv 40$ mJ/m^2. ($\alpha = 2.5 \times 10^{-3}$, times $\tau = 0, 0.30, 1.4, 3.4, 6.5, 11, 16$.)

lamination of opal-A does not fully develop (fig. 10B). Because, among other factors, the concentration varies according to the clay content the number of nuclei also varies with the clay distribution (fig. 10C). But this variation is indirect and therefore much weaker compared to the previous. The final result is a rather weak pattern in opal-CT, which carries the imprint of the initial distribution.

3.2.4. Case IV: Nucleation and pressure solution.—This case differs little from Case II. For the range of values considered, nucleation is a much stronger mechanism and overwhelms pressure solution (fig. 11). Better competition would arise if we were to reduce the interfacial energy dependence on clay content. However, this was not attempted. We conclude the following: Pressure solution significantly affects the pattern of the dissolving phase (amorphous) with diffusion strength controlling pattern development. As far as the precipitate pattern is concerned a key role is played by nucleation. If the latter is clay concentration-dependent, the pattern develops mostly in the regions of low clay content, according to the present model. If not, a balance between pressure solution and nucleation develops, such that the opal-CT pattern is "anti-symmetric" to the amorphous (fig. 10).

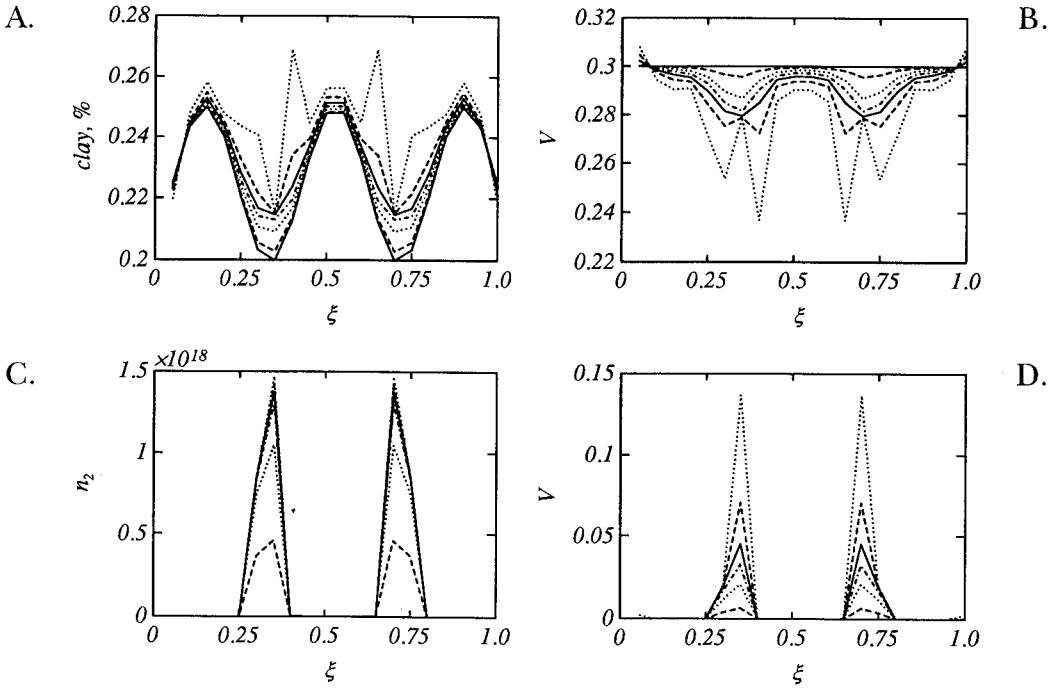

Fig. 11. Non-uniform nucleation with pressure solution. (A) Relative clay content; (B) opal-A content; (C) total nuclei density; (D) opal-CT content. ($\alpha = 2.5 \times 10^{-3}$, times $\tau = 0$, 0.30, 1.4, 3.4, 6.5, 11, 16, 23.)

4. PARTICLE COARSENING

The second effect taken to interpret lamination during silica diagenesis is particle coarsening. In a solution involving dissolving species, smaller solid particles are thermodynamically less stable than larger ones because of their larger specific surface area and correspondingly higher solubility. If nucleation does not terminate in a short time, the resulting crystals have a broad size distribution. As nuclei continue to grow, the supersaturation of the solution decreases. When the concentration in solution falls below the equilibrium concentration corresponding to smaller particles, the latter start dissolving to feed larger particles. This process is known as Ostwald ripening. In the one-dimensional formulation, where the material dissolved can be transported through diffusion or convection, particles, at different positions, can interact with each other. Then, larger particles consume not only smaller particles nearby but also those at some distance away. The resulting interaction gives rise to spatial patterns (Feeney and others, 1983). In this section, we explore this mechanism as a hypothesis for lamination in the diagnesis of silica (opal-A to opal-CT).

The system considered consists of species 1 (opal-A), species 2 (opal-CT), and silicic acid (H_4SIO_4), as described in eq (1). It is assumed that nucleation has ceased, so that species 2 only undergoes particle growth. Therefore, the number of dissolving and growing particle, N_1 and N_2, respectively remains constant. We denote by C the concentration of H_4SiO_4 and by ψ_1, ψ_2 the inverse of a specific surface area of the respective species. The appropriate mass balances become

$$\frac{\partial s}{\partial \tau} = \alpha\beta\psi_{10}\frac{\partial^2 s}{\partial \xi^2} - \beta\left(\nu_1\psi_1^2\frac{\partial \psi_1}{\partial \tau} + \nu_2\rho_r\psi_2^2\frac{\partial \psi_2}{\partial \tau}\right) \tag{37}$$

$$\frac{\partial \psi_1}{\partial \tau} = s - s_1^*(\psi_1); \tag{38}$$

$$\frac{\partial \psi_2}{\partial \tau} = \frac{1}{\rho_r}[s - s_2^*(\psi_2)C_r] \tag{39}$$

$$s_1^*(\psi_1) = \left(1 + \frac{2\psi_1^2}{2\psi_1^3 + \psi_{1c}^3}\right) \tag{40}$$

$$s_2^*(\psi_2) = 1 + \frac{2G_r\psi_2^2}{2\psi_2^3 + \psi_{2c}^3} \tag{41}$$

where we have additionally denoted

$$\nu_1 = N_1/(N_1 + N_2) \tag{42}$$

$$\nu_2 = N_2/(N_1 + N_2) \tag{43}$$

$$n_r = N_2/N_1 \tag{44}$$

$$G_r = \frac{\sigma_2}{\sigma_1}\frac{\rho_2}{\rho_1} = \sigma_r\rho_r \tag{45}$$

The above formulation was studied both analytically and numerically.

4.1. Linear Stability

We consider a spatially uniform solution, s_0, ψ_{10}, ψ_{20}, the stability of which to small perturbations is analyzed following normal modes

$$s = s_0 + \epsilon_1 \sin(n\pi\xi)\exp(\omega\tau) \tag{46}$$

$$\psi_1 = \psi_{1,0} + \epsilon_2 \sin(n\pi\xi)\exp(\omega\tau) \tag{47}$$

$$\psi_2 = \psi_{2,0} + \epsilon_3 \sin(n\pi\xi)\exp(\omega\tau). \tag{48}$$

Substitution into eqs (37) to (39) and linearization yields the following third order eigenvalue condition (Chang, 1991)

$$\begin{aligned}\rho_r\omega^3 + \omega^2[(\dot{s}_1^*\rho_r + \dot{s}_2^*(C_r) + \beta\psi_{10}^2\rho_r\alpha n^2\pi^2 + \beta\rho_r(\nu_1\psi_{10}^2 + \nu_2\psi_{20}^2)] \\ +\omega[\dot{s}_1^*\dot{s}_2^*C_r + \beta\psi_{10}^2\alpha n^2\pi^2(\dot{s}_1^*\rho_r + \dot{s}_2^*C_r) + \beta(\nu_1\psi_{10}^2C_r\dot{s}_2^* + \nu_1\rho_r\psi_{20}^2\dot{s}_1^*)] \\ + \beta\psi_{10}^2\alpha n^2\pi^2\dot{s}_1^*\dot{s}_2^*C_r = 0\end{aligned} \tag{49}$$

When the solubilities are independent of particle size for either phase, $\dot{s}_1^* = 0$ and $\dot{s}_2^* = 0$, the three roots are simply

$$\omega_1 = 0 \tag{50}$$

$$\omega_2 = 0 \tag{51}$$

$$\omega_3 = -\beta\psi_{10}^2(\nu_1 + \alpha n^2\pi^2 + \nu_2\psi_{10}^2/\psi_{20}^2) < 0 \tag{52}$$

This sytem is marginally stable, and spatial patterns will not form.

On the other hand, when particle size effects on solubility are considered, instabilities do develop. Here, it is more convenient to examine the large number wave behavior ($n \gg 1$). The system reduces to the quadratic

$$\omega^2 + \omega(\dot{s}_1^* + \dot{s}_2^* C_r/\rho_r) + \dot{s}_1^* \dot{s}_2^* C_r/\rho_r = 0 \tag{53}$$

with the following solution

$$\omega_1 = -\dot{s}_1^* \tag{54}$$

$$\omega_2 = -\dot{s}_2^* C_r/\rho_r \tag{55}$$

Given the solubility dependence eqs (40) and (41), both roots are positive, suggesting pattern formation. The first root, ω_1, expresses the tendency to layering due to dissolution, while the second, ω_2, the tendency due to growth. Note that the patterns are predicted to be independent of β.

4.2. Numerical Solution

To test the linear analysis results, we subsequently consider the full numerical solution. As initial conditions we take $\psi_1 = 3$, $\psi_2 = 1.23$, and both phases to be in equilibrium with the solution (fig. 12). A small magnitude perturbation (1 percent) on the particle sizes was imposed, the initial perturbations being either a single frequency sinusoidal or a multi-frequency fractional Brownian motion (fBm). Various parameter combinations of parameters were studied as shown in table 3. Particular emphasis was placed on effects of diffusion. In general, the process can be considered as occurring in two stages. The first stage is the complete dissolution of phase 1. During this step, both phases coexist, the amorphous continuously dissolving while ripening, while the second phase is growing. The length of this step is determined by the initial amount (particle size and population) of the amorphous phase. For a fixed particle size, a small value of n_r results in early depletion of phase 1 and vice versa. The second stage starts when the amorphous phase has been completely dissolved, and patterns occur only due to the ripening of phase 2. Sensitivity studies were carried out regarding the two parameters, β and n_r. Typical results are shown in figure 13. At early times, the pattern develops according to the initial disturbance (fig. 13A, B). After the dissolution of the amorphous phase, ripening of the second phase begins, the late time pattern acquires ripening features, which tend to obscure the original perturbation (fig. 13E).

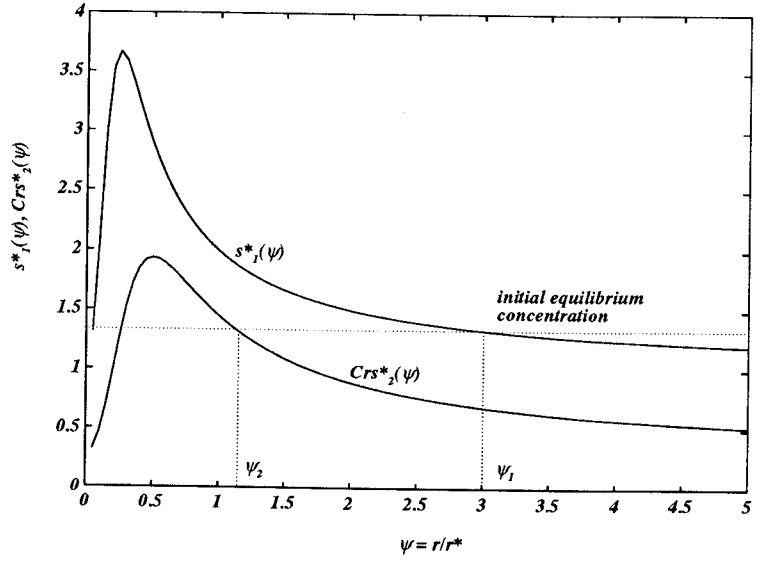

Fig. 12. Equilibrium solubility as a function of particle size for the two phases.

Results showed that the resulting patterns are identical both at early and late times for two widely different values of β (1, fig. 13 and 1000, fig. 14). This lack of sensitivity of β was predicted from linear analysis.

The effect of the ratio n_r was examined next. Different perturbations were used to carry out this investigation. For an fBm perturbation, the early results for either $n_r = 0.01$ (fig. 14) or $n_r = 1.0$ (fig. 15) differ little from each other, although in the latter case, depletion of phase 1 is faster. At the end of the first stage of the process, phase 2 still bears the pattern of phase 1. However, late-time results, when phase 1 is completely dissolved, are dramatically different. Because no more mass is available from the dissolution of phase 1, the growth of phase 2 at a given location will be at the expense of its own phase at other locations. Early-formed

TABLE 3

Parameter values for numerical calculations

Case	α	β	n_r	Perturbation
1	0.01	1	0.01	fBM
2	0.01	1000	0.01	fBm
3	0.01	1000	1.0	fBM
4	0.01	1000	0.01	sinusoidal, 0.5 cycles
5	0.01	1000	1.0	sinusoidal, 0.5 cycles
6	0.1	1000	1.0	fBM
7	2.5×10^{-3}	1000	1.0	fBM

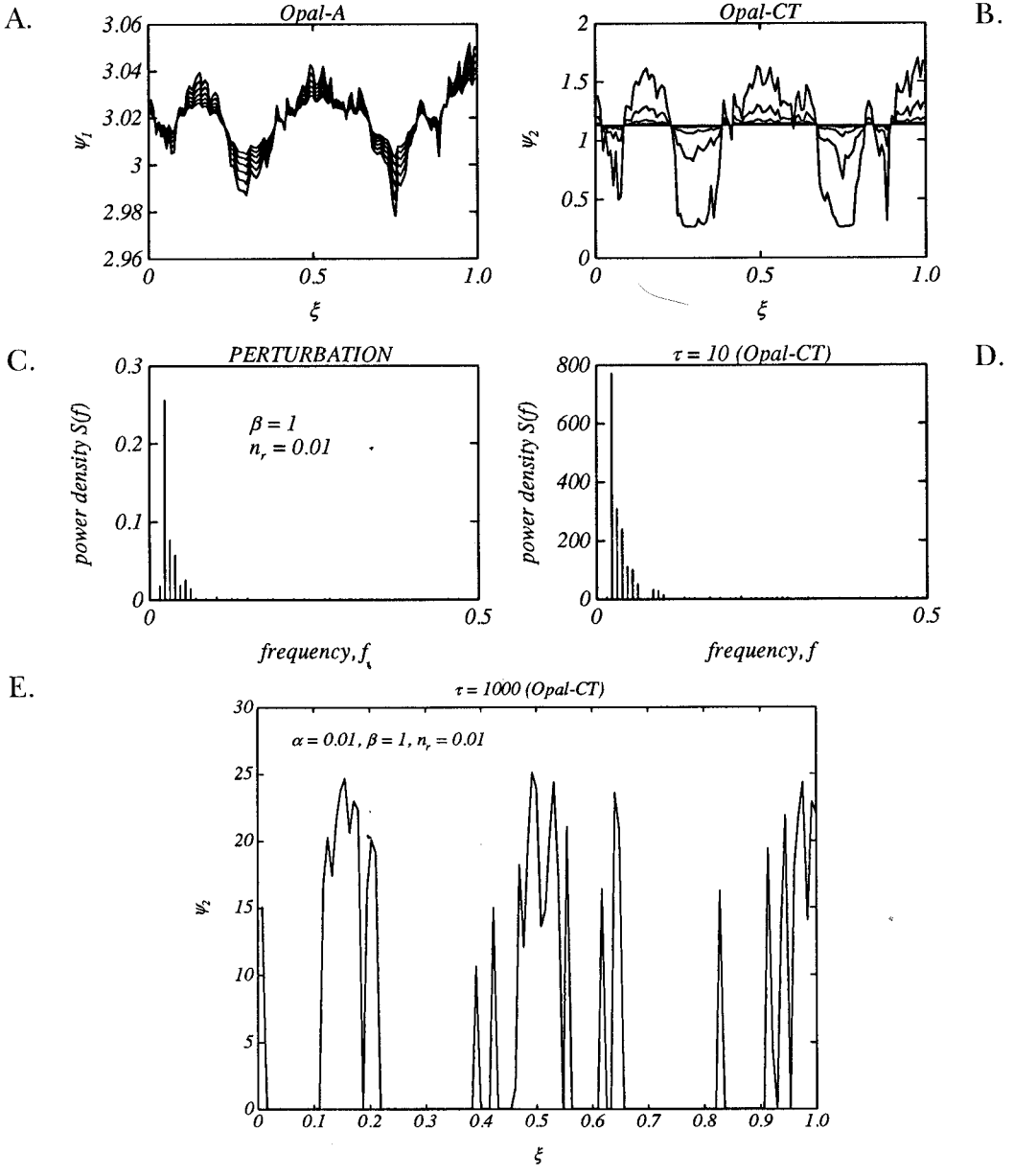

Fig. 13. Phase transformation and ripening for $\alpha = 0.01$, $\beta = 1$, and $n_r = 0.01$ (fBm perturbation). (A) Phase 1, (B) phase 2, (C) spectrum of initial perturbation, (D) spectrum of phase 2 at time $\tau = 10$, (E) late time result ($\tau = 1000$).

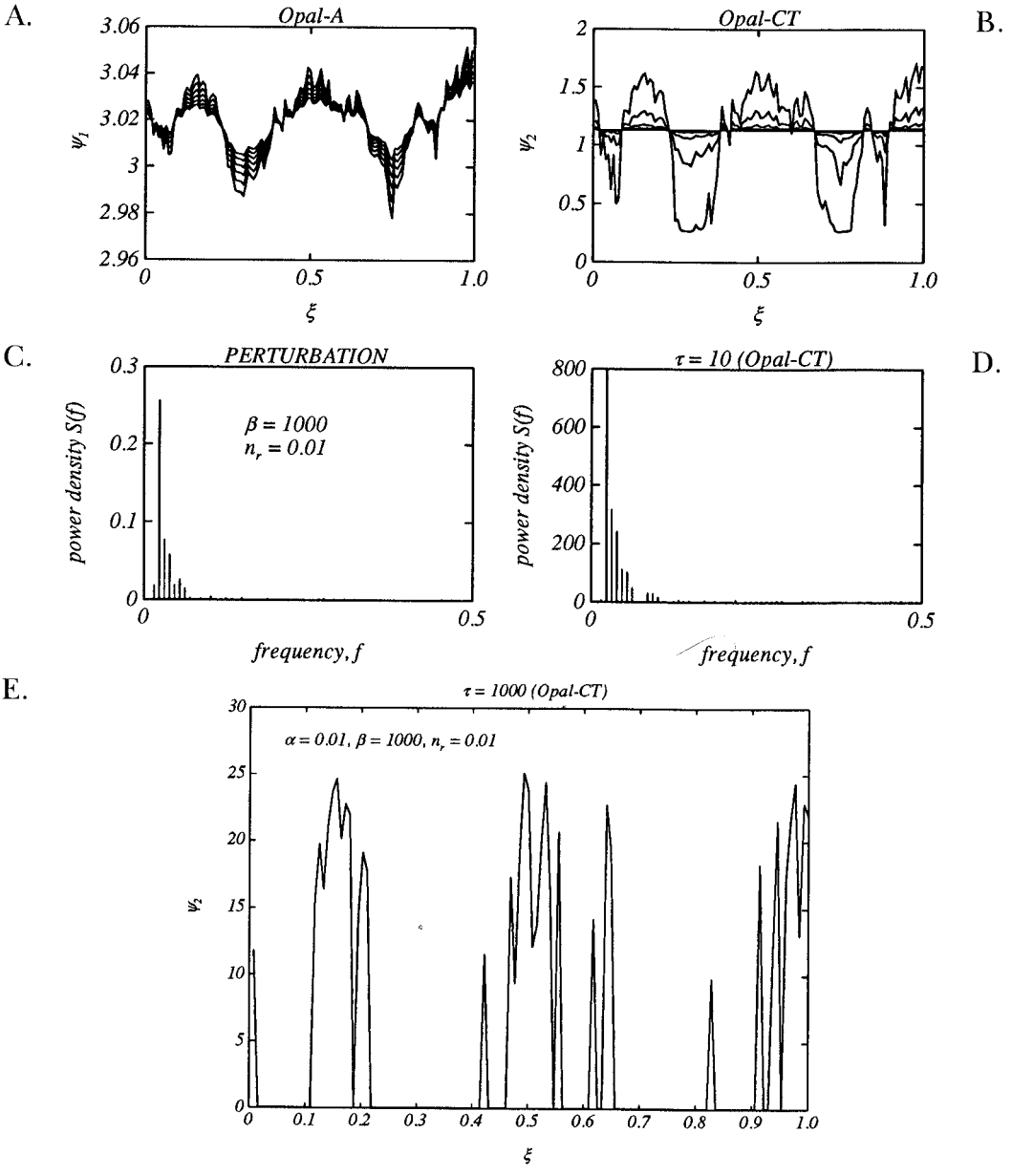

Fig. 14. Phase transformation and ripening for $\alpha = 0.01$, $\beta = 1000$, and $n_r = 0.01$ at time $\tau = 10$. (A) Phase 1, (B) phase 2, (C) spectrum of initial perturbation, (D) spectrum of phase 2, (E) phase 2 at time $\tau = 1000$.

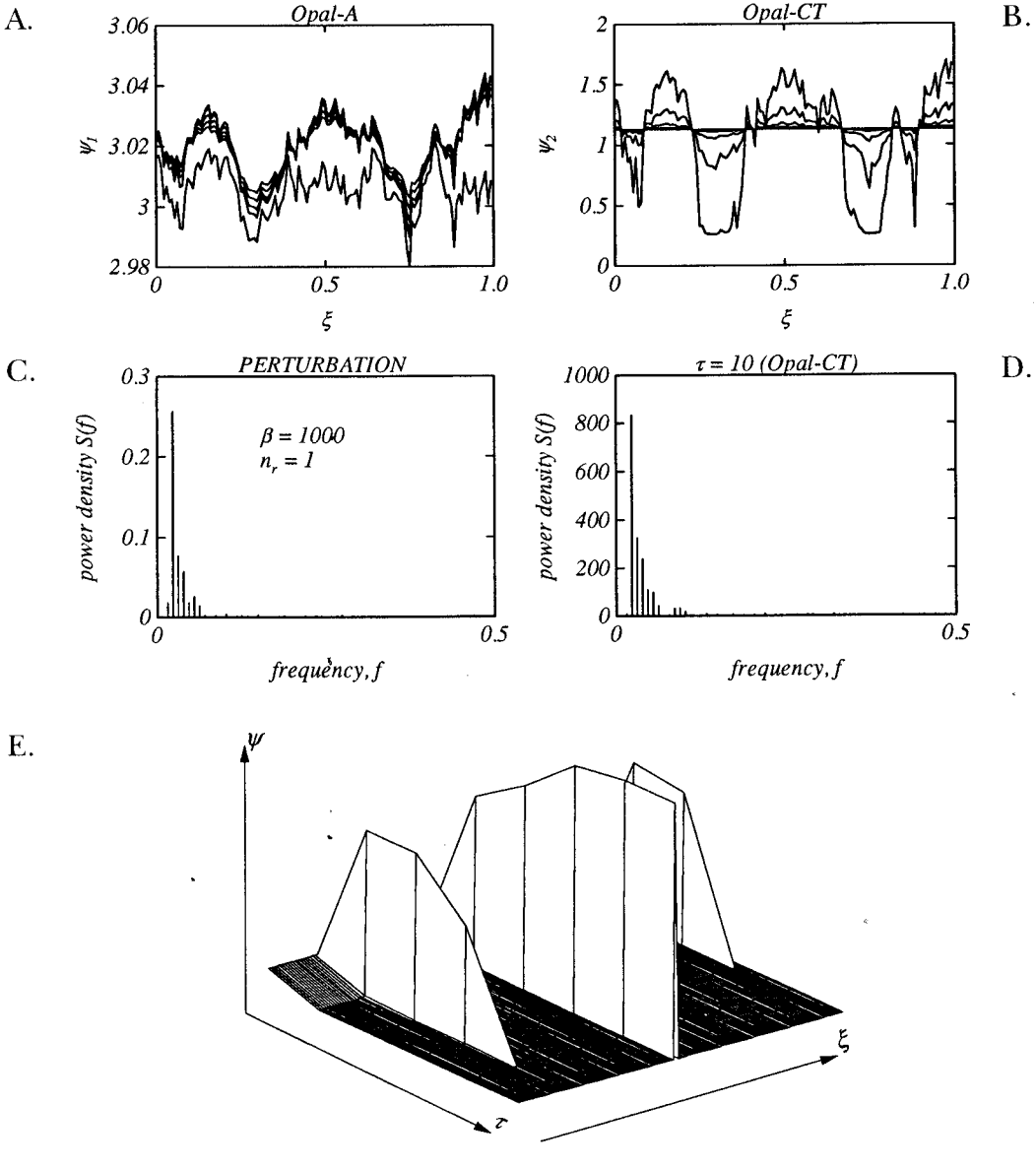

Fig. 15. Phase transformation and ripening for $\alpha = 0.01$, $\beta = 1000$, and $n_r = 1.0$ (fBm perturbation). (A) Phase 1, (B) phase 2, (C) spectrum of the perturbation and (D) spectrum of phase 2 at time $\tau = 10$, (E) phase 2 at late time $\tau = 1000$.

peaks near large particles now start to dissolve, resulting in lower frequency patterns. For $n_r = 0.01$, when phase one is completely dissolved, the size of phase 2 has reached a large value, additional ripening becomes very slow, and the high frequency features of the original perturbation are still evident (fig. 14E). For $n_r = 1.0$, however, the size of phase 2 is small when phase one is completely consumed, thus further ripening plays an important role in determining the final pattern. The end result is that the high frequency features of the original perturbations are completely lost (fig. 15E).

Similar results were obtained when the initial perturbation is a low frequency sinusoidal wave. The only difference is that for low values of n_r, the original *low* frequency feature is only partially inherited, while for larger values of n_r, this feature no longer exists (figs. 16E, 17E).

The effect of diffusion was considered by varying the parameter α by a factor of 400 (figs. 18 and 19). As expected, when diffusion is strong, the low frequency part of the initial perturbation is kept, although late time results indicate that initial peaks also tend to split further (fig. 18E). While for weaker diffusion, the short wavelength part of the initial variation is enhanced and kept even for large times (fig. 19E). The obvious difference is that the spacing between peaks is much larger in the case of strong diffusion than in the case of weak diffusion. In all the above, strong or weak diffusion is in relation to kinetics.

Both linear stability and numerical simulation results clearly demonstrate that the final lamination of phase 2 results from only a slight variation of phase 1. The lamination pattern of phase 2 may reflect exaggerated features of the original deposition, provided that the nucleation of phase 2 is a slow process. If significant numers of nuclei are generated, however, the final layering of the second phase appears to be totally unrelated to the original variations of phase 1. Short wavelength patterns are favored when diffusion is weak, or transformation (reaction) is fast, or the total surface area of phase 1 is large.

5. CONCLUDING REMARKS

In this paper, we formulated silica diagenesis as the phase transformation of opal-A to opal-CT in the presence of clay or other detrital materials. The two effects of clay suggested in the literature, namely pressure solution and the suppression of opal-CT nucleation, were considered. Linear stability and numerical results showed that small fluctuations in the amounts of clay, in conjunction with pressure solution and heterogeneous nucleation, are significant to trigger an instability that subsequently causes layer-like patterns during silica diagenesis. This mechanism requires only small initial variations either in amorphous or clay content, which, however, are enhanced manyfold during the process.

Diffusion is a key factor for the development of this mechanism of lamination. When it is slow compared to the kinetic rate, the dissolved solute is isolated and cannot be transported to other locations. The

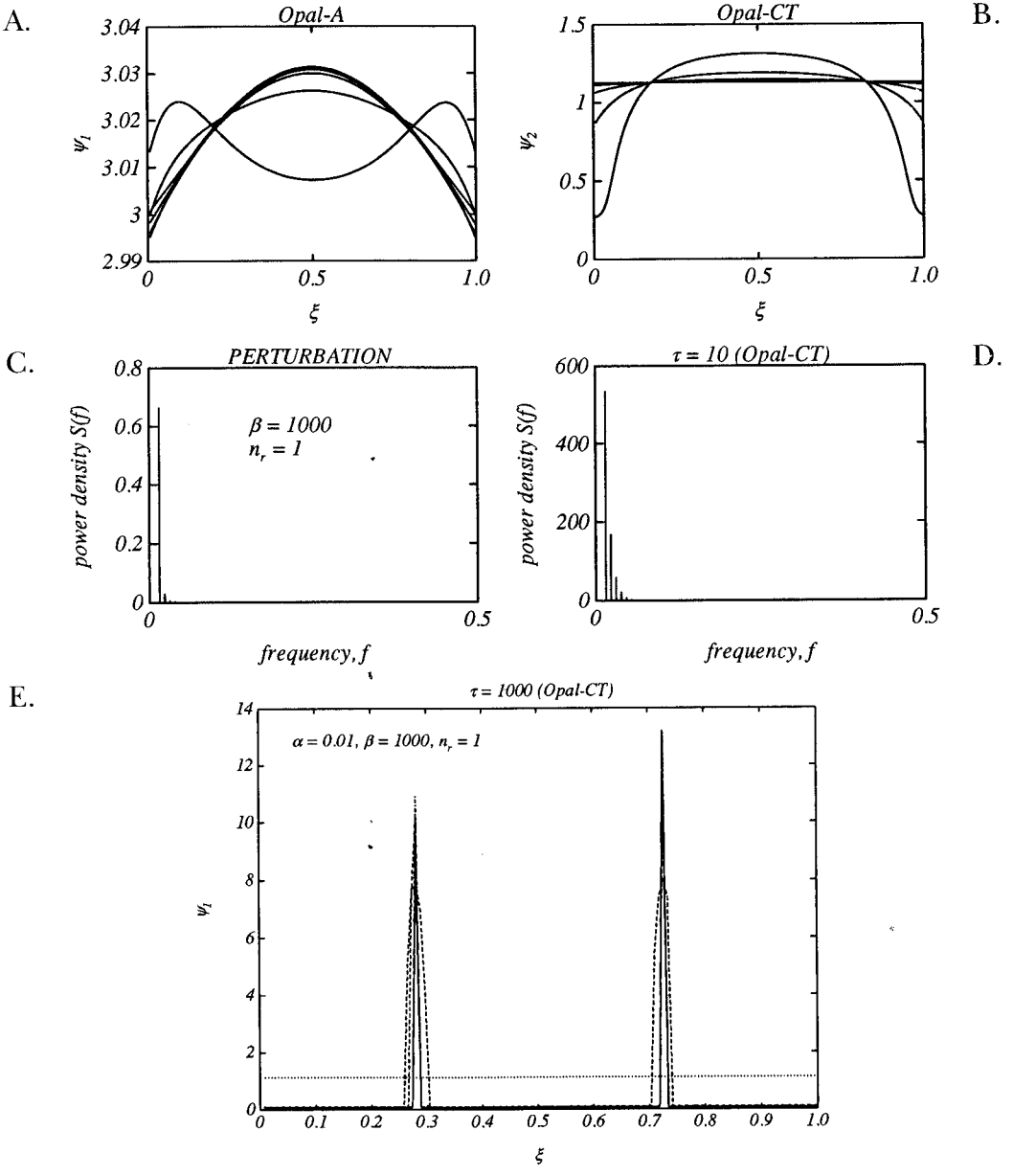

Fig. 16. Phase transformation and ripening for $\alpha = 0.01$, $\beta = 1000$, and $n_r = 0.01$ (sinusoidal perturbation) at times $\tau = 10$. (A) Phase 1, (B) phase 2, (C) spectrum of the perturbation, (D) spectrum of phase 2, (E) phase 2 at late time $\tau = 1000$.

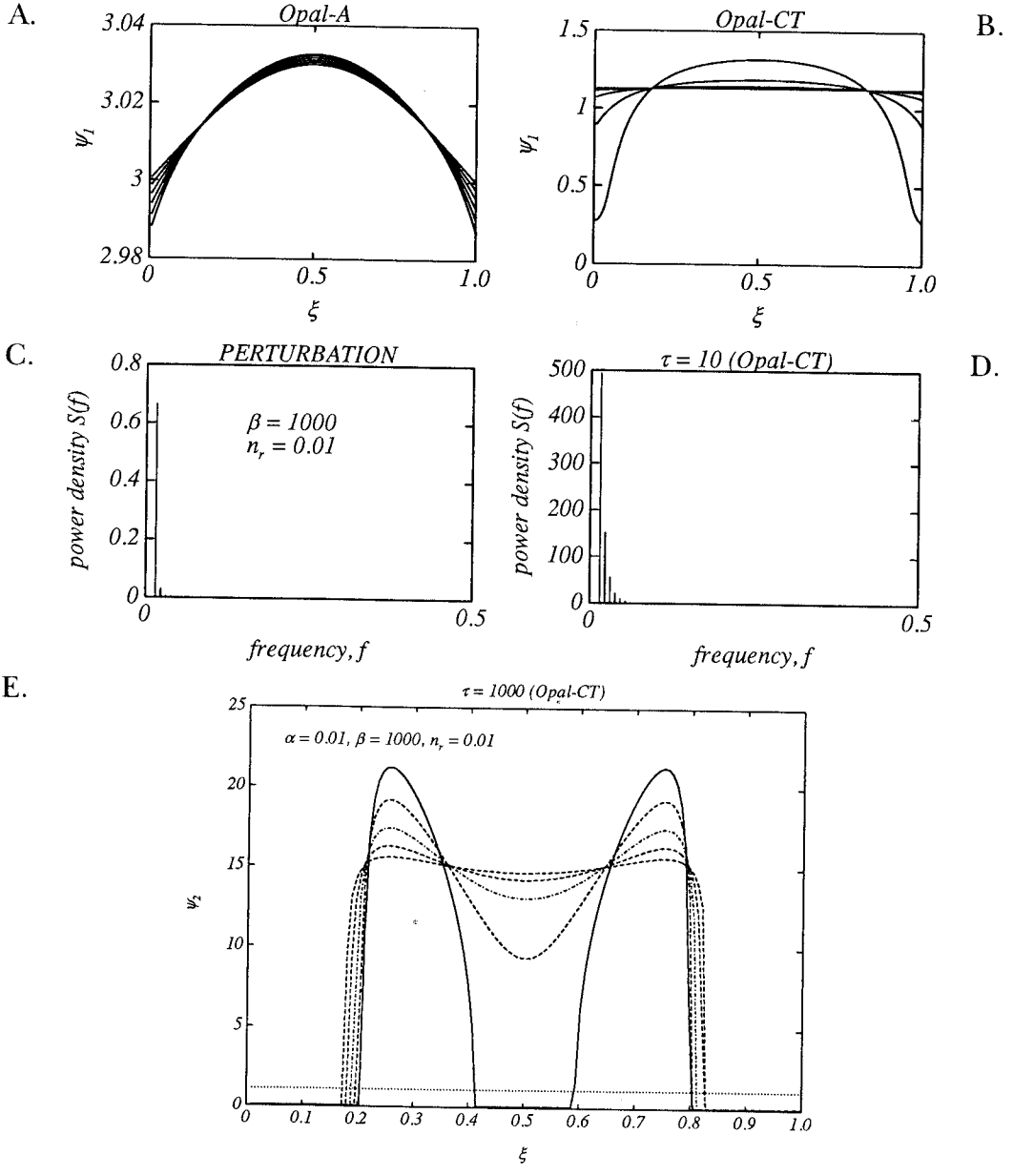

Fig. 17. Phase transformation and ripening for $\alpha = 0.01$, $\beta = .1000$, and $n_r = 1.0$ (sinusoidal perturbation) at time $\tau = 10$. (A) Phase 1, (B) phase 2, (C) spectrum of the perturbation, (D) spectrum of phase 2, (E) phase 2 at late time $\tau = 1000$.

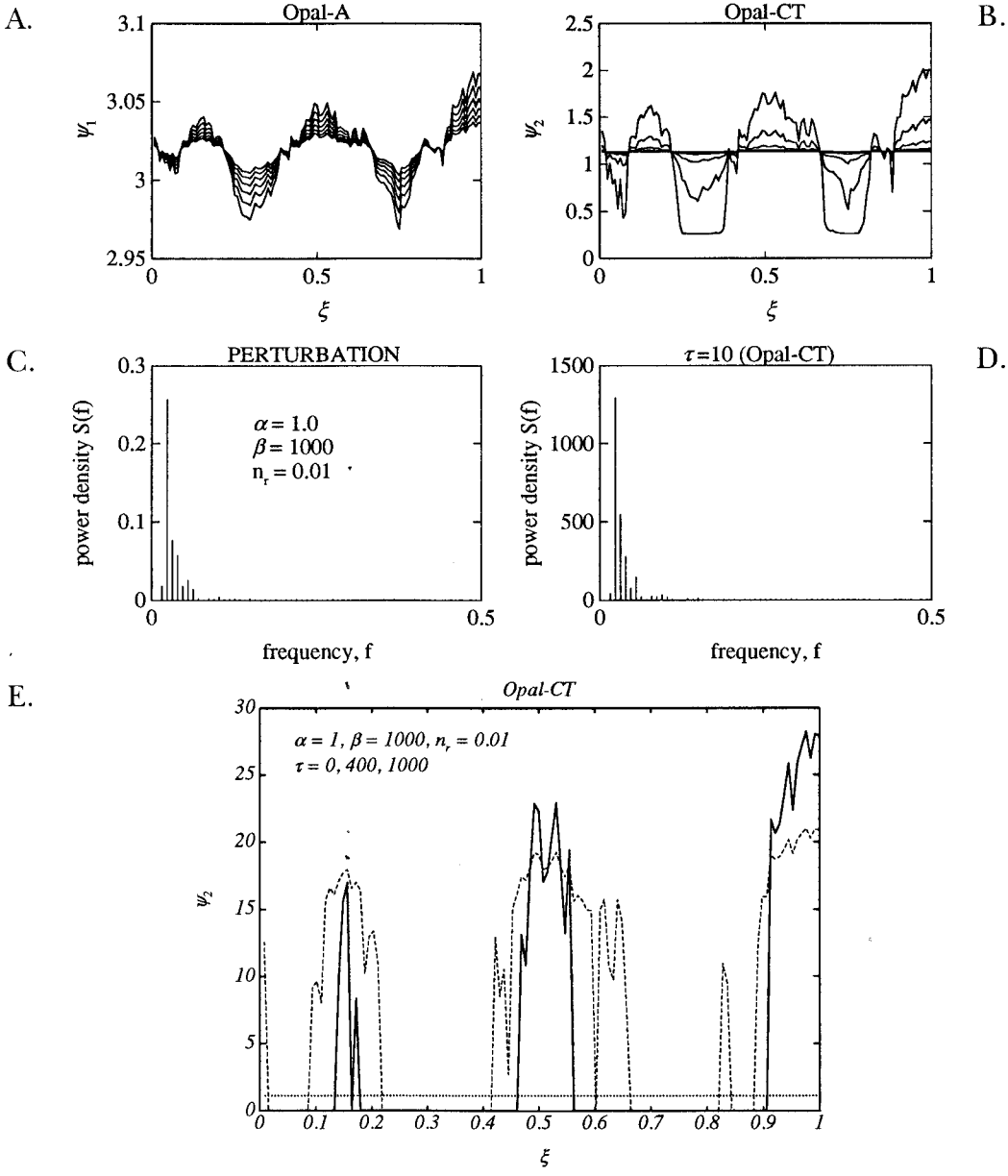

Fig. 18. Two-phase transformation and ripening for strong diffusion ($\alpha = 1.0$). (A) Phase 1, (B) phase 2, (C) spectrum of the perturbation, (D) spectrum of phase 2 at time $\tau = 10$, (E) phase 2 at late time (dotted, dashed, and solid lines are for times $\tau = 0$, 400, and 1000, respectively).

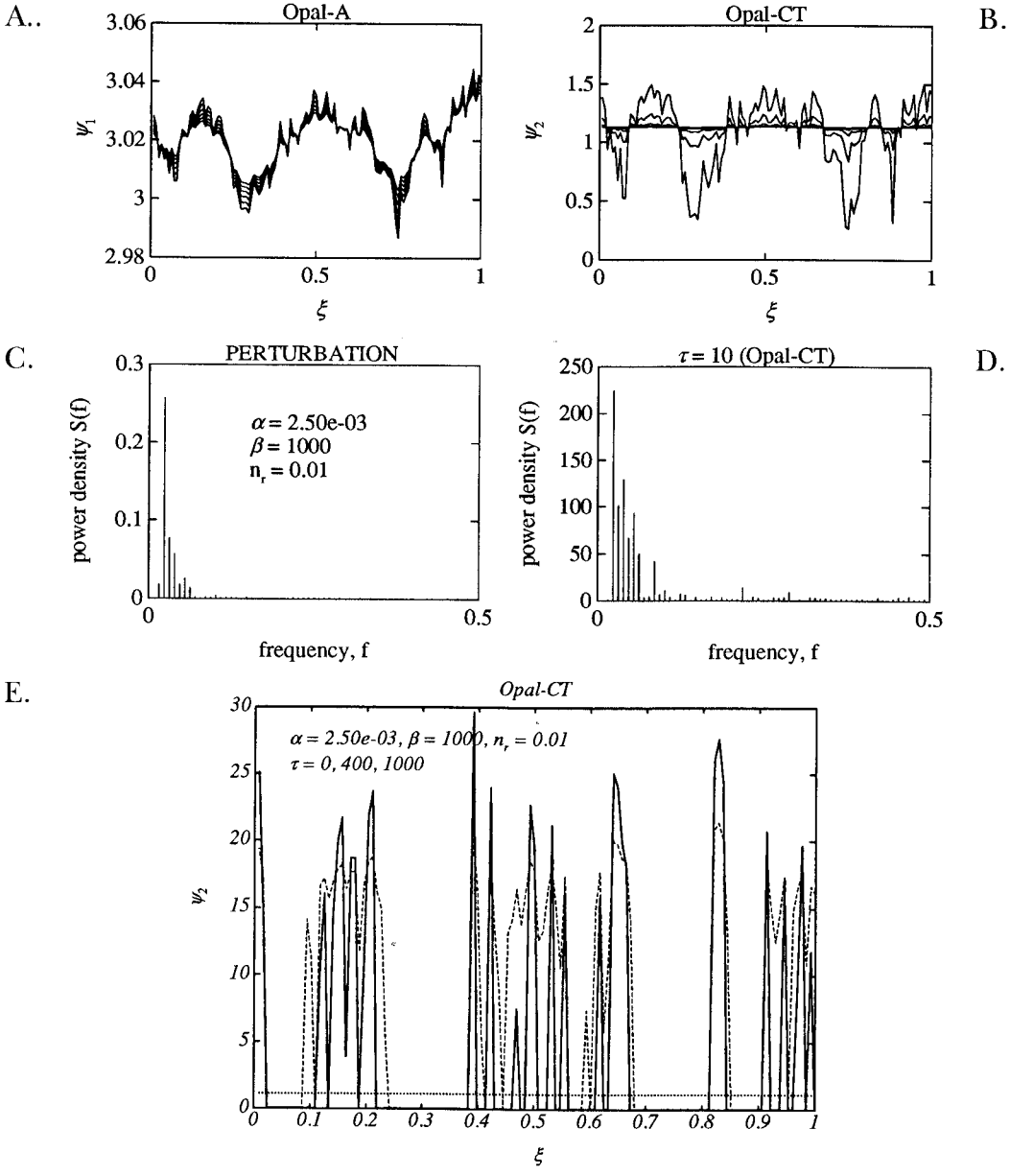

Fig. 19. Two-phase transformation and ripening for weak diffusion ($\alpha = 2.5 \times 10^{-3}$). (A) Phase 1, (B) phase 2, (C) spectrum of the perturbation, (D) spectrum of phase 2 at time $\tau = 10$, (E) phase 2 at late time (dotted, dashed, and solid lines are for times $\tau = 0$, 400, and 1000, respectively).

relative strengths of diffusion and dissolution/growth rates control the wavelength of the final pattern. Under the same perturbation, short wavelength layering was obtained for the case of weak diffusion, while long wavelength bedding results when diffusion is stronger.

Pressure solution was found to affect the dissolution of amorphous silica directly. When nucleation is also affected by the clay content, the precipitation of the second phase follows an "on-and off" sequence as the nucleation rate is highly sensitive to the variation of the interfacial tension with the detrital content. In this case, sharp contrast between each layer is expected. This effect is amplifying, rather than self-organizing.

For the case of particle size coarsening on two-phase transformation, ripening may occur for both phases at the same time. Then, the initial perturbation in phase 1 is transferred onto phase 2. Eventually, the amorphous phase will be consumed completely and phase 2 starts to ripen alone. The degree of such "post transformation ripening" depends on the size of phase 2 particles when the process is initiated. If the seeds of phase 2 are relatively few, when phase 1 is dissolved completely, ripening may be negligible, and the initial patterns in phase 1 may be partially kept in phase 2. On the other hand, if numerous crystalline seeds have been generated so that they have not grown fully when phase 1 is depleted, "post ripening" is expected to be significant, and the initial pattern completely fades away. Similar to the case of single phase, diffusion controls the spacing of the pattern with strong diffusion resulting in large spacing and vice versa.

The above two mechanisms may be used to interpret the microlamination observed during diagenesis of silica-rich formations such as the Monterey Formation. The theory above, although only applied to the opal-A to opal-CT reaction path, can be readily extended to the reaction opal-CT to quartz. Although plausible, its validity must await experimental and field verification. A useful step in the latter direction would be to compare theoretical and field frequency spectra in the laminated intervals.

ACKNOWLEDGMENTS

This work was supported in part by the University of Southern California Center for the Study of Fractured Reservoirs, Project "Monterey Formation." The contributions of the donor companies Conoco, Elf Aquitaine Petroleum, Oryx Energy Co., Phillips Petroleum, Shell Development Co., Texaco, and Unocal are gratefully acknowledged. We thank reviewers P. van Cappellen and C. I. Steefel for many useful suggestions.

REFERENCES

Berner, R. A., 1980. Early Diagenesis, A Theoretical Approach: Princeton, New Jersey, Princeton University Press, 241 p.

Bramlette, M. N., 1946, The Monterey Formation of California and the origin of its siliceous rocks: U.S. Geological Survey Professional Paper 212, 57 p.

Brueckner, H. K., Snyder, W. S., and Boudreu, M., 1987, Diagnetic controls on the structural evolution of siliceous sediments in the Golconda Allochthon, Nevada, USA: Journal of Structural Geology, v. 9, p. 403–417.

Chang, J., ms, 1991, Modeling of Microlamination and Flow in the Monterey Formation: Application of Self-Organization, Heterogeneity and Fractal Concepts: Ph. D. thesis, University of Southern California, Los Angeles, California, 192 p.

de Boer, R. B., 1977, On the thermodynamics of pressure solution—interaction between chemical and mechanical forces: Geochimica et Cosmochimica Acta, v. 41, p. 249–256.

de Boer, R. B., Nagtegaal, P. J. C., and Duyvis, E. M., 1977, Pressure solution experiments on quartz sand: Geochimica et Cosmochimica Acta, v. 41, p. 257–264.

Dee, G. T., 1986, The patterns produced by precipitation at a moving reaction front: Physica, 23D, p. 304–344.

Dunham, J. B., and Blake, G. H., 1987, Guide to coastal outcrops of the Monterey formation of western Santa Barbara County, California: Los Angeles, California, Society of Economic Paleontologists and Mineralogists, Pacific Section, Technical Report 53, 36 p.

Feder, J., 1988, Fractals: New York, Plenum Press, 283 p.

Feeney, R., Schmidt, S. L., Strickkolm, Chadam, P. J., and Ortoleva, P., 1983, Periodic precipitation and coarsening waves: Applications of the competitive particle growth model: Journal of Chemical Physics, v. 78, p. 1293–1311.

Fliker, M., and Ross, J., 1974, Mechanism of chemical instability for periodic precipitation phenomena: Journal of Chemical Physics, v. 60, p. 3458–3465.

Hurd, D. C., 1983, Physical and chemical properties of siliceous skeletons, *in* Aston, S. R., editor, Silicon Geochemistry and Biogeochemistry: London and New York, Academic Press, p. 187–244.

Hurst, H. E., 1951, Long-term storage capacity of reservoirs: Transactions of American Society of Civil Engineering, v. 116, p. 770.

Iler, R. K., 1979, The Chemistry of Silica: New York, John Wiley & Sons, 866 p.

Isaacs, C. M., ms, 1980, Diagenesis in the Monterey Formation Examined Laterally Along the Coast Near Santa Barbara, California: Ph.D. thesis, Stanford University, Stanford, California, 329 p.

———— 1981, Porosity reduction during diagenesis of the Monterey formation, Santa Barbara coastal area, California, *in* Garrison, R. E., and Douglas, R. G., editors, The Monterey formation and related siliceous rocks of California: Los Angeles, California, Society of Economic Paleontologists and Mineralogists, Pacific Section, p. 257–271.

———— 1982, Influence of rock composition on kinetics of silica phase changes in the Monterey formation, Santa Barbara area, California: Geology v. 10, 304–308.

———— 1983, Compositional variation and sequence in the Miocene Monterey formation, Santa Barbara area, California, in Larue, D. K., and Steel, R. J., editors, Cenozoic marine sedimentation: Pacific Margin, U.S.A.: Los Angeles, California, Society of Economic Paleontologists and Mineralogists, Pacific Section, p. 117–132.

———— 1984a, Geology and physical properties of the Monterey formation, California: paper SPE 12733 presented at the Society of Petroleum Engineers California Regional Meeting held in Long Beach, California, April 11–13, 1984.

———— 1984b: The Monterey-key to offshore California boom: Oil & Gas Journal, p. 75–81.

Kastner, M., Keene, J. B., and Gieskes, J. M., 1977, Diagenesis of siliceous oozes–I. chemical controls on the rate of opal-A to opal-CT transformation—an experimental study: Geochimica et Cosmochimica Acta, v 41,p. 1041–1059.

Keller, J. B., 1980, Liesegang Rings and Theory of Fast Reaction and Slow Diffusion, *in* Stewart, W. E., Ray, W. H. Conley, C. C., editors, Dynamics and modelling of reactive systems: New York, Academic Press, p. 211–224.

———— 1981, Recurrent precipitation and Liesegang rings: Journal of Chemical Physics, v. 74, p. 5000–5007.

Lapidus, L., and Amundson, N. R., editors, 1977, Chemical Reactor Theory, A Review: Englewood Cliffs, New Jersey, Prentice-Hall, 552 p.

Mandelbrot, B. B., and van Ness, J. W., 1968, Fractional Brownian motions, fractional noises, and applications: SIAM Review, v. 10, p. 422–437.

Mandelbrot, B. B., and Wallis, J. R., 1969, Some long-run properties of geophysical records: Water Resource Research, v. 5, p. 321–340.

Morse, J. W., and Casey, W. H., 1988, Ostwald processes and mineral paragenesis in sediments: American Journal of Science, v. 288, p. 537–560.

Ortoleva, P., 1983, The self organization of Liesegang bands and other precipitate patterns, *in* Nicolis, G., and Baras, F., editors, Chemical Instabilities, (NATO ASI Series C: Mathematical and Physical Science): Boston, D. Reidel Publishing Company, p. 290–297.

Ortoleva, P., Chadam, J., Merino, E., and Sen, A., 1987a, Geochemical self-organization II: The reactive-infiltration instability: American Journal of Science, v. 287, p. 1008–1040.
Ortoleva, P., Merino, E., Moore, C., and Chadam, J., 1987b, Geochemical self-organization I: Reaction-transport feedbacks and modeling approach: American Journal of Science, v. 287, p. 979–1007.
Pisciotto, K. A., and Garrison, R. E., 1981, Lithofacies and depositional environments of the Monterey formation, *in* Garrison, R. E. and Douglas, R. G., editors, The Monterey formation and related siliceous rocks of California: Los Angeles, California, Society of Economic Paleontologists and Mineralogists, Pacific Section, p. 97–122.
Rimstidt, J. C., and Barnes, H. L., 1980, The kinetics of silica-water reactions: Geochimica et Cosmochimica Acta, v. 44, p. 1683–1699.
Sharma, M. M., and Yortsos, Y. C., 1987, Transport of particulate suspensions in porous media: Model formulation: American Institute of Chemical Engineers Journal, v. 33, p. 1636–1643.
Steefel, C. I., and van Cappellen, P., 1990, A new kinetic approach to modeling water-rock interaction: The role of nucleation, precursors, and Ostwald ripening: Geochimica et Cosmochimica Acta, v. 54, p. 2657–2677.
Stern, K. H., 1954, The Liesegang phenomenon: Chemistry Reviews, v. 54, p. 79–99.
Venzl, G., 1986a, Pattern formation in precipitation processes. I. The theory of competitive coarsening: Journal of Chemical Physics, v. 85, p. 1996–2005.
———— 1986b, Pattern formation in precipitation processes. II. A postnucleation theory of Liesegang bands: Journal of Chemical Physics, v. 85, p. 2006–2011.
Venzl, G., and Ross, J., 1982 Nucleation and colloidal growth in concentration gradients, (Liesegang rings): Journal of Physical Chemistry, v. 77, p. 1302–1307.
Walton, A. G., 1967, The Formation and Properties of Precipitates: New York, Interscience Publishers, 232 p.
Williams, L. A., and Crerar, D. A., 1985, Silica diagenesis, II. General mechanisms: Journal of Sedimentary Petrology, v. 55, p. 312–321.
Williams, L. A., Parks G., and Crerar, D. A., 1985, Silica diagenesis, I. Solubility controls: Journal of Sedimentary Petrology, v. 55, p. 301–311.